Unique morphogenetic signatures define mammalian neck muscles and associated connective tissues

Eglantine Heude[1,2], Marketa Tesarova[3], Elizabeth M. Sefton[4], Estelle Jullian[5], Noritaka Adachi[5], Alexandre Grimaldi[1,2], Tomas Zikmund[3], Jozef Kaiser[3], Gabrielle Kardon[4], Robert G. Kelly[5] and Shahragim Tajbakhsh[1,2]

[1] Department of Developmental & Stem Cell Biology, Institut Pasteur, France

[2] CNRS UMR 3738, Paris, France

[3] Central European Institute of Technology, Brno University of Technology, Czech Republic

[4] Department of Human Genetics, University of Utah, Salt Lake City, USA

[5] Aix-Marseille Université, CNRS UMR 7288, IBDM, Marseille, France

* To whom correspondence should be addressed:

Dr. Shahragim Tajbakhsh

Department of Developmental & Stem Cell Biology, CNRS UMR 3738

Institut Pasteur

25, rue du Dr. Roux

75015 Paris, France

email: shahragim.tajbakhsh@pasteur.fr

Tel: +33 1 40 61 35 20

Fax: +33 1 45 68 89 63

ABSTRACT

In vertebrates, head and trunk muscles develop from different mesodermal populations and are regulated by distinct genetic networks. Neck muscles at the head-trunk interface remain poorly defined due to their complex morphogenesis and dual mesodermal origins. Here, we use genetically modified mice to establish a 3D model that integrates regulatory genes, cell populations and morphogenetic events that define this transition zone. We show that the evolutionary conserved cucullaris-derived muscles originate from posterior cardiopharyngeal mesoderm, not lateral plate mesoderm, and we define new boundaries for neural crest and mesodermal contributions to neck connective tissue. Furthermore, lineage studies and functional analysis of *Tbx1*- and *Pax3*-null mice reveal a unique genetic program for somitic neck muscles that is distinct from that of somitic trunk muscles. Our findings unveil the embryological and developmental requirements underlying tetrapod neck myogenesis and provide a blueprint to investigate how muscle subsets are selectively affected in some human myopathies.

INTRODUCTION

The neck is composed of approximately 80 skeletal muscles in humans that allow head mobility, respiration, swallowing and vocalization processes, containing essential elements such as the trachea, esophagus, larynx, and cervical vertebrae. These processes are ensured by a robust network of muscles at the head-trunk interface, a transition zone subjected to a spectrum of human muscle diseases such as dropped head syndrome, oculopharyngeal myopathy, myotonic dystrophy, Duchenne-type dystrophy and congenital muscular disorders (Emery, 2002; Martin et al., 2011; Randolph and Pavlath, 2015). Defining the embryology of these distinct muscle groups is critical to understand the mechanisms underlying the susceptibility of specific muscles to muscular dystrophies. While myogenesis at the cranial and trunk levels has been studied extensively, the developmental mechanisms at the basis of neck muscle formation are poorly documented and often debated (Ericsson et al., 2013).

In vertebrates, head and trunk muscles arise from different mesodermal origins and their development depends on distinct myogenic programs. At the cranial level, the cardiopharyngeal mesoderm (CPM) resides in pharyngeal arches and gives rise to branchiomeric muscles and the second heart field. Myogenic specification of the CPM is initiated by the activation of genes such as *Mesp1*, *Islet1* and *Tbx1*, while *Pax7* subsequently marks muscle stem cells (Diogo et al., 2015; Kelly et al., 2004; Nathan et al., 2008; Saga et al., 1996; Sambasivan et al., 2009). In contrast, *Pax3* and *Pax7* expression in the somitic mesoderm gives rise to trunk and limb muscles, with *Pax3* then being downregulated in most muscles during foetal stages, while *Pax7* maintains the stem cell pool (Kassar-Duchossoy et al., 2005; Relaix et al., 2005 ; Tajbakhsh et al., 1997). After the differential specification of cranial and trunk progenitors, the bHLH myogenic regulatory factors (MRFs) Myf5, Mrf4, Myod and Myog regulate myogenic cell fate and differentiation (reviewed in (Comai and Tajbakhsh, 2014; Noden and Francis-West, 2006)).

In early embryos, *Tbx1* is required for robust activation of MRF genes and proper branchiomeric muscle formation (Grifone et al., 2008; Kelly et al., 2004; Kong et al., 2014; Sambasivan et al., 2009). In *Tbx1* mutant embryos, the first pharyngeal arch is hypoplastic and posterior pharyngeal arches do not form resulting in variably penetrant defects of masticatory muscles and absence of muscles derived from more posterior arches (Kelly et al., 2004; Lescroart et al., 2015; Theis et al., 2010). In humans, *TBX1* is a major gene involved in 22q11.2 deletion syndrome (DiGeorge/velo-cardio-facial syndrome), a congenital disease characterized by cardiovascular defects and craniofacial malformations (Papangeli and Scambler, 2013). In contrast, *Pax3* acts upstream of MRF genes in somites and *Pax3* mutants have defects of epaxial and hypaxial muscle formation while double *Pax3/Pax7*-null embryos lack trunk/limb muscles (Brown et al., 2005; Relaix et al., 2005; Tajbakhsh et al., 1997; Tremblay et al., 1998).

The neck constitutes a transition zone characterising land vertebrates (tetrapods). The major muscle groups in the neck consist of: epaxial back muscles; ventral hypaxial musculature; pharyngeal, laryngeal and esophagus striated muscles located medioventrally; and cucullaris-derived muscles. The cucullaris is a generic term defining putative homologous muscles that are evolutionarily conserved and connect the head and trunk in jawed vertebrates (gnathostomes). In amniotes, the cucullaris represents the embryonic anlage that gives rise to trapezius and sternocleidomastoid muscles which are innervated by the accessory nerve XI (Diogo, 2010; Edgeworth, 1935; Ericsson et al., 2013; Kuratani, 2008; Kuratani et al., 2018; Lubosch, 1938; Tada and Kuratani, 2015).

While the somitic origin of epaxial/hypaxial neck muscles and CPM origin of pharyngeal, laryngeal and esophagus striated muscles are well defined (Gopalakrishnan et al., 2015; Noden,

1983; Tabler et al., 2017), the embryological origin of cucullaris-derived muscles has remained a subject of controversy (Couly et al., 1993; Edgeworth, 1935; Greil, 1913; Huang et al., 1997; Huang et al., 2000; Matsuoka et al., 2005; Noden, 1983; Piatt, 1938; Piekarski and Olsson, 2007). This muscle group was reported to originate either from lateral plate mesoderm (LPM) or CPM populations adjacent to the first three somites in chick and axolotl (Nagashima et al., 2016; Sefton et al., 2016; Theis et al., 2010). However, retrospective lineage analysis indicated that the murine trapezius and sternocleidomastoid muscles are clonally related to second heart field-derived myocardium and laryngeal muscles, consistent with a CPM origin (Lescroart et al., 2015). Moreover, cucullaris development follows a branchiomeric program and cucullaris-derived muscles were reported to be absent in *Tbx1*-null mice (Kelly et al., 2004; Lescroart et al., 2015; Sefton et al., 2016; Theis et al., 2010). Nevertheless, the source of the cucullaris is still equivocal due to the location of its embryonic anlagen at the interface of cranial, somitic and lateral plate mesodermal populations.

Skeletal elements and muscle-associated connective tissue (MCT) also have distinct embryological origins along the rostro-caudal axis. The connective tissue of branchiomeric and tongue muscles originate from neural crest cells (NCCs) of cranial origin (Evans and Noden, 2006; Kontges and Lumsden, 1996; Noden, 1983, 1988; Ziermann et al., 2018b). Cranial NCCs also give rise to skeletal components and tendons in the head. In contrast, the skeleton and connective tissue originate from the somitic mesoderm in the trunk and from the LPM in limbs (Nassari et al., 2017). The neck and shoulder girdle contain skeletal elements and connective tissues of distinct NCC, LPM or somitic origins (Durland et al., 2008; Matsuoka et al., 2005; McGonnell et al., 2001; Nagashima et al., 2016; Tabler et al., 2017; Valasek et al., 2010). It has been suggested that NCCs form both connective tissue and endochondral cells at the attachment sites of neck muscles to shoulders in mouse (Matsuoka et al., 2005). However, studies in non-

mammalian animals have contested a NCC contribution to the pectoral girdle (Epperlein et al., 2012; Kague et al., 2012; Ponomartsev et al., 2017).

Therefore, the neck region consists of muscle, skeletal and connective tissue elements of mixed cellular origins, underscoring the difficulty in assigning embryonic identities for these structures. In addition, the genetic requirements for the formation of non-somitic and somitic neck muscles remain to be defined. To resolve these issues, we used genetic lineage and loss of function mice combined with histology, µCT and 3D reconstructions to map the embryological origins of all neck muscles and associated connective tissues. In doing so, we show that cucullaris-derived muscles originate from a posterior CPM population and are differentially affected in *Tbx1*-null mice. Moreover, we identify a unique genetic network involving both *Mesp1* and *Pax3* genes for somite-derived neck muscles and we define a new limit of neural crest contribution to neck connective tissue and shoulder components.

RESULTS

Distinct myogenic programs define neck muscle morphogenesis

To investigate the embryological origin of neck muscles in mouse, we mapped CPM- and somite-derived myogenic cells using lineage-specific *Cre* drivers including *Mef2c-AHF*, *Islet1*, *Mesp1* and *Pax3* (Figure 1). The *Mef2c-AHF* (anterior heart field) enhancer is activated in the second heart field and myogenic progenitors of CPM origin (Lescroart et al., 2010; Verzi et al., 2005). *Islet1* and *Mesp1* genes are both expressed during branchiomeric specification and are essential for cardiac development. The *Mesp1* lineage also marks some anterior somitic derivatives (Cai et al., 2003; Harel et al., 2009; Saga et al., 2000; Saga et al., 1999). In contrast, *Pax3* is activated in all somitic progenitors (Relaix et al., 2005; Tajbakhsh et al., 1997; Tremblay et al., 1998). Given that the majority of *Mef2c-AHF* derivatives are myogenic cells (Lescroart et al., 2015; Lescroart et al., 2010; Verzi et al., 2005), we analysed this lineage using $Rosa26^{R\text{-}lacZ/+}$ (*R26R*) reporter mice. *Islet1*, *Mesp1* and *Pax3* genes are also expressed in cells contributing to skeletal components, connective tissues or neurons. To focus on the myogenic lineage, we used $Pax7^{nGFP\text{-}stop/nlacZ}$ ($Pax7^{GPL}$) reporter mice, which mark cells with nuclear β-galactosidase (β-gal) activity following *Cre* recombination (Sambasivan et al., 2013).

We first examined embryos after myogenic specification (E10.5 and E11.75), and foetuses when muscles are patterned (E18.5). In $Mef2c\text{-}AHF^{Cre};R26R$ embryos, β-gal-positive cells were observed in the mesodermal core of pharyngeal arches at the origin of branchiomeric muscles, in second heart field derivatives, and in the cucullaris anlage (Figure 1A, E). A spatiotemporal analysis of the cucullaris using $Myf5^{Cre};Pax7^{GPL}$ and $Myf5^{Cre};R26^{mTmG}$ embryos (Figure 1-figure supplement 1) showed that *Myf5*-derived muscle progenitors located at the level of the posterior pharyngeal arches, and adjacent to somites S1-S3 (Figure 1-figure supplement 1A'), were innervated by the accessory nerve XI (Figure 1-figure supplement 1G-G"). These cells gave rise to

the trapezius and sternocleidomastoid muscles (Figure 1-figure supplement 1A-F') thus confirming the identity of the cucullaris anlage in mouse (Tada and Kuratani, 2015).

In *Islet1*^{Cre};*Pax7*^{GPL} and *Mesp1*^{Cre};*Pax7*^{GPL} embryos, labelling was also observed in pharyngeal arch derivatives and the cucullaris (Figure 1B-C, F-G), the latter showing less contribution from the *Islet1* lineage. On sections, only a subset of the Myod-positive cells in the cucullaris originated from *Islet1*-derived cells (Figure 1-figure supplement 2A). Surprisingly, *Pax3*^{Cre};*Pax7*^{GPL} embryos also showed *lacZ* expression in the cucullaris at E11.75, although no expression was detected at E10.5 (Figure 1D, H). Given that *Pax3* and *Pax7* are also expressed in neural crest cells (Relaix et al., 2004), and that these *Pax3*-derived cells were not positive for Myod expression (Figure 1-figure supplement 2B), they are likely to be of NCC origin. As expected, *Pax3* lineage tracing also labelled the somite-derived myotomes, hypaxial migrating progenitors that form the hypoglossal cord (origin of tongue and infrahyoid muscles), and limb muscle progenitors. Furthermore, the hypaxial anlage, which is located at the proximal limb bud and gives rise to the cutaneous maximus and latissimus dorsi muscles, was *Pax3*-derived (Figure 1D, H; Figure 1-figure supplement 1D') (Prunotto et al., 2004; Tremblay et al., 1998). Unexpectedly, this anlage and the latissimus dorsi muscle were also labelled in *Islet1*^{Cre};*Pax7*^{GPL} but not in *Mesp1*^{Cre};*Pax7*^{GPL} embryos (Figure 1F-G, J-K). On sections at E12.5, Islet1 expression was observed after the emergence of myogenic cells from the proximal limb bud (Figure 1-figure supplement 2C). In addition, the *Mesp1* lineage contributed to anterior somitic derivatives during early embryonic development as previously reported (Loebel et al., 2012; Saga et al., 1999); strong *lacZ* expression was observed in the hypoglossal cord and somites S1-S6. Labelling subsequently decreased in more posterior myotomes and in forelimb muscle progenitors compared to *Pax3*^{Cre};*Pax7*^{GPL} embryos (Figure 1C-D, G-H).

Lineage tracings with *Mef2c-AHF*^{Cre}, *Islet1*^{Cre} and *Mesp1*^{Cre} marked branchiomeric (temporal, masseter, digastric, mylohyoid and pharyngeal) and cucullaris-derived neck muscles (acromiotrapezius, spinotrapezius and sternocleidomastoid), all of which were excluded from the *Pax3* lineage (Figure 1I-L, Figure 1-figure supplement 2D-G'). These findings support previous studies showing that the cucullaris-derived muscles use a branchiomeric program (Kelly et al., 2004; Lescroart et al., 2015; Sefton et al., 2016; Theis et al., 2010). In addition, both *Mesp1* and *Pax3* lineages labelled somitic neck muscles (Figure 1 K-L', Figure 1-figure supplement 2F-G') indicating that the *Mesp1* lineage contributes to neck muscles to a larger extent than previously reported (Figure 1K-K', Figure 1-figure supplement 2F-F') (Harel et al., 2009).

To further investigate the contributions of *Mesp1* and *Pax3* lineages to neck muscles, we examined sections using the *R26*^{tdTomato} reporter co-immunostained with the myofibre marker Tnnt3 at three representative levels (A, B and C levels in Figure 1; see also Figure 2-figure supplement 1). At anterior levels, while *Pax3* lineage contribution was limited to somite-derived neck muscles, the *Mesp1* lineage marked branchiomeric muscles (mylohyoid, pharyngeal, laryngeal, esophagus), cucullaris-derived muscles (acromiotrapezius and sternocleidomastoid) and somite-derived neck muscles (Figure 2A-H, Figure 1-figure supplement 2F-G', Figure 2-figure supplement 2A-H'). The epaxial and hypaxial neck muscles showed equivalent Tomato expression in both *Mesp1*^{Cre}*;R26*^{tdTomato} and *Pax3*^{Cre}*;R26*^{tdTomato} mice. These observations indicate that *Mesp1* and *Pax3* lineages contribute equivalently to neck muscles derived from anterior somites.

At the shoulder level, we observed less *Mesp1* contribution to more posterior somitic muscles (Figure 2I-J). In contrast to that observed at anterior levels, little or no Tomato expression was detected in myofibres of scapular muscles in *Mesp1*^{Cre}*;R26*^{tdTomato} mice (Figure 2-figure

supplement 2I-J'). Therefore, *Mesp1* lineage contribution was restricted to epaxial and hypaxial somite-derived neck muscles in contrast to pectoral and trunk muscles that originate from the *Pax3* lineage (Figures 1-2) (Table 1). These observations lead us to propose that 3 distinct myogenic programs are involved in the formation of neck and pectoral musculature at the head-trunk interface. The branchiomeric and cucullaris-derived muscles depend on a common myogenic program involving *Mef2c-AHF*, *Islet1* and *Mesp1* lineages; the somitic neck muscles that originate from anterior somites derive from both *Mesp1* and *Pax3* lineages; the pectoral muscles derived from more posterior somites depend on the activation of *Pax3* only (Table 1).

Dual neural crest and mesodermal origins of neck connective tissues

To define the cellular origin of neck muscle-associated connective tissue (MCT), we traced the contribution of different embryonic populations using $Mesp1^{Cre};R26^{tdTomato}$ and $Pax3^{Cre};R26^{tdTomato}$ mice as well as $Wnt1^{Cre}$ and $Prx1^{Cre}$ reporters that label NCC and postcranial LPM derivatives respectively (Burke and Nowicki, 2003; Danielian et al., 1998; Durland et al., 2008). Both NCC and LPM populations were reported to participate to trapezius MCT (Durland et al., 2008; Matsuoka et al., 2005). Moreover, it was suggested that the postcranial LPM is a source for cucullaris-derived muscles (Theis et al., 2010). A direct comparison of NCC and LPM derivatives allowed us to clarify the contribution of these two populations to cucullaris formation (Figures 3-4).

We first investigated the distribution of neck muscles and NCCs using $Myf5^{nlacZ/+}$, *Mef2c-*AHF^{Cre}*;R26R*, $Pax3^{Cre}$*;R26R* and $Wnt1^{Cre}$*;R26R* embryos (Figure 3-figure supplement 1). At E10.5, the cucullaris anlage was positioned at the level of posterior pharyngeal arches where *Wnt1*-derived positive cells were detectable (Figure 1A-C, Figure 1-figure supplement 1A', Figure 3-figure supplement 1A-B). Subsequently, the cucullaris progenitors expanded caudally from

E11.5 to E13.5. The posterior limit of the cranial NCC domain also extended posteriorly, however the *Wnt1*-labelled cells did not cover the posterior portion of cucullaris-derived muscles (Figure 3-figure supplement 1C-H). At E14.5, the acromiotrapezius and spinotrapezius attained their definitive position in *Myf5*$^{nlacZ/+}$ and *Mef2c-AHF*^{Cre}*;R26R* embryos (Figure 3-figure supplement 1I-J). *Wnt1*-derived cells were observed in the anterior acromiotrapezius muscle, but not in the spinotrapezius that was situated in a *Pax3*-derived domain (Figure 3-figure supplement 1K-L). Analysis of whole-mount embryos indicated that the cranial NCCs did not contribute to connective tissue of posterior cucullaris derivatives, in contrast to what was reported previously (Matsuoka et al., 2005).

To further analyse NCC contribution to the cervical region at the cellular level, we performed immunostainings on sections for Tomato and Tnnt3 in E18.5 *Wnt1*^{Cre}*;R26*^{tdTomato} foetuses (Figure 3, Figure 3-figure supplement 2). Given that the *Wnt1* lineage is a source of both neuronal and connective tissue derivatives, we associated Tomato immunostaining with Tuj1 that marks neuronal cells and with Tcf4 that labels MCT fibroblasts (Figure 3, Figure 3-figure supplements 2-3). At the cranial level, the MCT of branchiomeric (masseter, mylohyoid) and tongue muscles was derived from *Wnt1*- and *Pax3*-lineages but not from the mesodermal *Mesp1* lineage (Figure 3-figure supplement 2A-B', Figure 3-figure supplement 3A, F, Figure 3-figure supplement 4A-B, E). The acromiotrapezius showed a high contribution from *Wnt1*-derived cells while the underlying epaxial muscles had considerably less labelled cells that were limited to the neuronal Tuj1-positive population (Figure 3A-A'). The *Wnt1* lineage gave rise to Tcf4-positive fibroblasts in the acromiotrapezius, but not in epaxial neck muscles, where fibroblasts were derived from the *Mesp1* lineage (Figure 3-figure supplements 3B-C, 4C). These observations are in accordance with a NCC origin of branchiomeric, trapezius and tongue connective tissue as reported previously (Matsuoka et al., 2005).

However, the NCC contribution to connective tissue in the sternocleidomastoid subset of cucullaris-derived muscles appeared more heterogeneous than that observed in the acromiotrapezius. In rodents, the sternocleidomastoid is composed of three individual muscles (cleidomastoid, sternomastoid and cleido-occipitalis portions); a differential NCC contribution to MCT was observed in these muscles. While *Wnt1*-derived NCCs were widely present in the sternomastoid and cleido-occipitalis, the NCC contribution was limited in the cleidomastoid (Figure 3B-B'). Indeed, Tcf4-positive fibroblasts in the cleido-occipitalis originated from the *Wnt1* lineage whereas the majority of MCT fibroblasts in the cleidomastoid were derived from the *Mesp1* lineage (Figure 3-figure supplements 3D-E, 4D).

A differential contribution of NCCs to connective tissue was also seen within the laryngeal and infrahyoid musculature. Extensive *Wnt1* lineage contributions to MCT was observed in laryngeal muscles (thyroarytenoid and cricothyroid) that connect to the thyroid cartilage, which is of NCC origin (Figure 3C-C') (Tabler et al., 2017). In contrast, the laryngeal muscles (cricoarytenoid and vocal muscles) that link mesoderm-derived laryngeal cartilages (cricoid, arytenoid and medio-caudal portion of the thyroid) did not contain NCC-derived connective tissue (Figures 2G-H, 3C-C') (Tabler et al., 2017). In these muscles, the *Wnt1*-derived cells were neuronal, as observed in the esophagus, whereas the MCT fibroblasts were derived from the *Mesp1* lineage (Figure 3C-C', Figure 3-figure supplements 2D-D', 4F). As another example, *Wnt1*-derived cells contributed to a greater extent to MCT in infrahyoid muscles (thyrohyoid muscles) that connect the hyoid and thyroid cartilage that are of NCC origin, compared to infrahyoid muscles (omohyoid and sternohyoid muscles) that link posteriorly pectoral structures of mesodermal origin (Figure 3-figure supplement 2C, C', H; Figure 3-figure supplement 3G-H). These observations suggest that MCT composition within laryngeal and infrahyoid muscles correlates in part with the embryonic

origin of the skeletal components to which they attach (Figure 2G-H, Figure 3C-C', Figure 3-figure supplement 2C-C', H).

Given our findings that connective tissues of neck muscles have differential contributions of NCC and mesodermal populations, we analysed the caudal connections of the cucullaris-derived muscles to the pectoral girdle (Figure 3D, Figure 3-figure supplement 2E-H). The acromiotrapezius attaches dorsally to the nuchal ligament and ventrally to the scapular acromion process in continuity with the scapular spine. While *Wnt1*-derived cells were present dorsally (Figure 3A, Figure 3-figure supplement 2E), this contribution diminished gradually and was undetectable at the insertion on the scapula (Figure 3D-D', Figure 3-figure supplement 2F). Similarly, the sternocleidomastoid muscle showed limited NCC contribution to the attachment sites of the clavicle and sternum (Figure 3-figure supplement 2G-H). In contrast to what was previously described (Matsuoka et al., 2005), we did not observe NCC contribution to the shoulder endochondral tissue nor to the nuchal ligament (Figure 3-figure supplement 2E-H). Taken together, these observations define a novel boundary for neural crest contribution to neck/pectoral components. The posterior contribution limit of branchiomeric MCT occurs at the level of laryngeal muscles that connect to NCC skeletal derivatives. Moreover, NCCs do not participate in connecting posterior cucullaris and infrahyoid muscles to their skeletal elements.

To assess the cellular origin of cucullaris connective tissue at posterior attachment sites, we next traced the contribution of lateral plate mesoderm (LPM) to the neck/shoulder region using *Prx1*^{Cre} reporter mice (Durland et al., 2008; Logan et al., 2002) (Figure 4, Figure 4-figure supplements 1-2). Analysis of E9.5 embryos showed that *Prx1*-derived cells contribute to the forelimb bud and cells adjacent to the anterior-most somites (Figure 4A). At E12.5, the postcranial *Prx1*-derived domain clearly defined the lateral somitic frontier along the rostrocaudal axis (Durland et al.,

2008) and did not include the cucullaris anlage (Figure 4-figure supplement 1, white arrowheads). Whole-mount immunostainings for the myogenic markers Pax7/Myod/My32 and for GFP in *Prx1*^{Cre};*R26*^{mTmG} embryos showed that *Prx1*-derived cells were present in the dorsal part of the cucullaris but did not contribute to myofibres (Figure 4B, white arrowheads). At E18.5, the *Prx1* lineage marked the limb, scapular and abdominal regions, whereas only a few *Prx1*-derived cells were detected in the cucullaris-derived sternocleidomastoid, acromiotrapezius and spinotrapezius muscles (Figure 4C-D). On sections, immunostaining for β-gal and Tnnt3 showed that *Prx1*-derived LPM contributed to limb/shoulder MCT and to skeletal components of the pectoral girdle (Figure 4E, Figure 4-figure supplement 2A-B). In contrast, fewer *Prx1*-derived cells were detected in the acromiotrapezius and little or no contribution was observed in the epaxial muscles (Figure 4E, Figure 4-figure supplement 2B-C). In addition, only a limited number of *Prx1*-derived cells gave rise to Tcf4-positive fibroblasts in the trapezius muscles, but they contributed more extensively to the fibroblast population in scapular muscles (Figure 4F-F'', white arrowheads, Figure 4-figure supplement 2D-D"). Notably, β-gal expression for this lineage was not detected in trapezius myofibres thereby confirming the results obtained at E12.5 (Figure 4B-F", Figure 4-figure supplements 1-2).

Therefore, these observations reveal a dual NCC/LPM origin of trapezius connective tissue, with a decrease of NCC contribution at posterior attachment sites. Moreover, our analysis shows that the postcranial LPM does not give rise to cucullaris myofibres in contrast to what was suggested previously (Theis et al., 2010), thus providing further evidence for a branchiomeric origin of the cucullaris.

330 **Divergent functions of *Tbx1* and *Pax3* in neck development**

331 Given the key role for *Tbx1* and *Pax3* genes in the specification of the CPM and somites
332 respectively, we analysed the effect of inactivation of these genes on neck muscle formation
333 compared to the muscle phenotypes observed at cranial and trunk levels. Analysis has been
334 performed by immunostainings on sections and 3D reconstructions of the neck and pectoral girdle
335 using high resolution micro-computed tomographic (µCT) scans of control, *Tbx1*$^{-/-}$ and *Pax3*$^{-/-}$
336 foetuses (Figures 5-6).

337

338 Analysis of *Tbx1* mutants revealed unexpected features in cucullaris and hypaxial neck muscle
339 formation. As previously described (Gopalakrishnan et al., 2015; Kelly et al., 2004), anterior
340 branchiomeric muscles (digastric and mylohyoid) showed phenotypic variations, whereas
341 posterior branchiomeric muscles (esophagus and intrinsic laryngeal muscles) and the
342 acromiotrapezius were severely affected or undetectable (Figure 5B, E, H; Figure 6B) (Table 2).
343 However, detailed examination of the cucullaris-derived muscles revealed a heterogeneous
344 dependence on *Tbx1* function that was not reported previously (Lescroart et al., 2015; Theis et al.,
345 2010). Unexpectedly, the sternocleidomastoid muscle was present bilaterally but smaller (Figure
346 6B); the different portions (cleido-occipitalis, cleidomastoid and sternomastoid) were unilaterally
347 or bilaterally affected in a stochastic manner. Moreover, while the epaxial neck and scapular
348 muscles were unaffected (Figure 5E, Figure 6E-H), the hypaxial neck muscles derived from
349 anterior somites were altered. Indeed, the tongue and longus capitis were reduced and the
350 infrahyoid and longus colli muscles were severely affected or undetectable (Figure 5B, H, Figure
351 6E, H; see interactive 3D PDFs in Rich Media Files 1-2).

352

353 Analysis of *Pax3* mutants showed that the neck and pectoral muscles were differentially affected.
354 As expected, the branchiomeric and epaxial muscles developed normally but displayed

355 morphological differences adapted to malformations noted in some skeletal components (Figure
356 5C, F; Figure 6C, I). However, whereas hypaxial trunk/limb muscles were severely affected or
357 undetectable in *Pax3* mutants (Figure 5F, I; Figure 6 F, I) (Tajbakhsh et al., 1997; Tremblay et al.,
358 1998), surprisingly the majority of hypaxial neck muscles derived from both *Mesp1* and *Pax3*
359 lineages were present. Tongue muscles were reduced in size but patterned, the infrahyoid were
360 hypoplastic, whereas the longus capitis and longus colli were unaffected (Figure 5C; Figure 6F, I;
361 see interactive 3D PDF in Rich Media File 3). The phenotypes of the different muscle groups
362 observed in *Tbx1* and *Pax3* mutants are summarized in Table 2.
363
364 Taken together, these observations revealed that hypaxial muscles in the neck were less affected in
365 *Pax3* mutants than more posterior hypaxial muscles, pointing to distinct requirements for *Pax3*
366 function during neck and trunk muscle formation. In addition, *Tbx1* mutants exhibited more severe
367 phenotypes in hypaxial neck muscles, thus highlighting distinct roles for this gene in
368 branchiomeric and hypaxial neck myogenesis.
369

DISCUSSION

The embryological origins of neck muscles and connective tissues at the head-trunk interface have been poorly defined largely due to their localisation at a transition zone that involves multiple embryonic populations. Using a combination of complementary genetically modified mice and 3D analysis that identifies muscles in the context of their bone attachments, we provide a detailed map of neck tissue morphogenesis and reveal some unexpected features regarding the muscle and connective tissue network.

Branchiomeric origin of cucullaris-derived muscles

The mammalian neck consists of somitic epaxial/hypaxial muscles, branchiomeric muscles and cucullaris-derived muscles (Table 1). The latter constitute a major innovation in vertebrate history, connecting the head to the pectoral girdle in gnathostomes and allowing head mobility in tetrapods (Ericsson et al., 2013). Recent studies in different organisms including shark, lungfish and amphibians suggest that the cucullaris develops in series with posterior branchial muscles and that its developmental origin is conserved among gnathostomes (Diogo, 2010; Naumann et al., 2017; Noda et al., 2017; Sefton et al., 2016; Ziermann et al., 2018a; Ziermann et al., 2017). However, multiple embryological origins including CPM, LPM and somites have been reported for the cucullaris, underscoring the difficulty in deciphering the morphogenesis of this and other muscles in the head-trunk transition zone (Huang et al., 2000; Nagashima et al., 2016; Sefton et al., 2016; Theis et al., 2010).

Our studies show that the cucullaris anlage is innervated by the accessory nerve XI (Tada and Kuratani, 2015) and develops contiguously with the mesodermal core of posterior arches and anterior-most somites 1-3. Our lineage analysis reveals that cucullaris development depends on a branchiomeric myogenic program involving *Mef2c-AHF*, *Islet1* and *Mesp1* lineages in keeping

with previous results (Table 1) (Lescroart et al., 2015; Sefton et al., 2016; Theis et al., 2010). However, our detailed 3D reconstructions and functional analysis lead us to modify the view of the genetic requirements of cucullaris-derived muscles (Lescroart et al., 2015; Theis et al., 2010). Notably, these muscles are differentially affected in *Tbx1*-null foetuses; the acromiotrapezius does not form while the sternocleidomastoid is present but reduced. Therefore, *Tbx1* is differentially required for sternocleidomastoid and trapezius formation, suggesting that distinct subprograms regulate cucullaris development.

We also demonstrate that the cucullaris anlage is excluded from the postcranial *Prx1*-derived expression domain, which instead gives rise to connective tissue, thereby excluding contribution from LPM to cucullaris-derived myofibres. Thus, our results, combined with grafting experiments in chick and axolotl (Nagashima et al., 2016; Sefton et al., 2016), suggest that the postcranial extension of the CPM lateral to the first three somites in tetrapod embryos is a source of cucullaris myogenic cells (Figure 7A). The discordance with previous studies regarding the origin of the cucullaris is likely due to its proximity to both anterior somites and LPM (Figure 7A-B), and consequently, to potential contamination of embryonic sources in grafting experiments (Couly et al., 1993; Huang et al., 1997; Huang et al., 2000; Noden, 1983; Piekarski and Olsson, 2007; Theis et al., 2010).

A unique genetic program for somite-derived neck muscles

Our study also points to a unique *Mesp1*/*Pax3* genetic program in anterior somites for epaxial/hypaxial neck muscle formation (Table 1). While it was shown that the *Mesp1* lineage gives rise to tongue muscles (Harel et al., 2009), we demonstrate that it also contributes to all neck muscles. In chordates, *Mesp* genes appear to play a conserved role in cardiogenesis and axis segmentation. In mouse, *Mesp1* inactivation causes early embryonic death from abnormal heart

development, and *Mesp1/Mesp2* double-knockout embryos lack non-axial mesoderm (Moreno et al., 2008; Saga, 1998; Saga et al., 2000; Satou et al., 2004; Sawada et al., 2000). During early murine development, *Mesp1* shows two waves of activation; initially in the nascent mesoderm destined for extraembryonic, cranial and cardiac mesoderm at the onset of gastrulation; later during somitogenesis, transient *Mesp1* expression is limited to anterior presomitic mesoderm (Saga, 1998; Saga et al., 1996; Saga et al., 2000; Saga et al., 1999). Our lineage analysis shows that *Mesp1* extensively labels the anterior mesoderm, including the CPM and anterior somites 1-6, while contribution decreases in more posterior somites (Loebel et al., 2012; Saga et al., 2000; Saga et al., 1999). Furthermore, we show that *Mesp1*-derived anterior somites give rise to all epaxial/hypaxial neck muscles in contrast to trunk/limb muscles originating from more posterior somites marked by *Pax3*. The boundary of *Mesp1* lineage contribution to muscles corresponds to the neck/pectoral interface. Our findings suggest that the anterior somitic mesoderm employs a specific "transition program" for neck muscle formation involving both *Mesp1* and *Pax3* genes implicated in CPM and somitic myogenesis respectively (Figure 7A-C).

Whereas little is known about the function of *Mesp* genes in chordates, there is evidence that *Mesp1* might be differentially required during anterior *versus* posterior somitic formation. In mouse, different *Mesp1* enhancer activities have been observed between CPM/anterior somites and posterior somites indicating that the regulation of *Mesp1* expression might differ in the two embryonic compartments (Haraguchi et al., 2001). In zebrafish, quadruple mutants of *Mesp* genes (*Mesp-aa/-ab/-ba/-bb*) lack anterior somite segmentation while the positioning of posterior somite boundaries is unaffected, suggesting distinct requirements for *Mesp* genes in anterior and posterior somites (Yabe et al., 2016). Interestingly, during early ascidian development, *Mesp* is expressed in B7.5 founder cells that give rise to both CPM and anterior tail muscles (ATM) (Satou et al., 2004). In *Ciona*, the CPM precursors at the origin of heart and atrial siphon (pharyngeal) muscles depend

445 on the ascidian homologs of *Mesp1*, *Islet1* and *Tbx1* (reviewed in (Diogo et al., 2015)), indicating
446 that a conserved genetic network promotes chordate myogenesis in the anterior embryonic
447 domain.
448
449 Our lineage analysis also reveals an unexpected contribution of *Islet1*-derived cells to the
450 formation of cutaneous maximus and latissimus dorsi muscle progenitors (Table 1) (Prunotto et
451 al., 2004; Tremblay et al., 1998). *Islet1* is activated in a subset of CPM progenitors giving rise to
452 branchiomeric muscles and second heart field myocardium (Cai et al., 2003; Harel et al., 2009;
453 Nathan et al., 2008). At the trunk level, while *Islet1* is widely expressed in the nervous system and
454 in the LPM forming the hindlimb bud (Cai et al., 2003; Yang et al., 2006), to our knowledge its
455 expression in somitic myogenic cells has not been reported. The cutaneous maximus and
456 latissimus dorsi muscles are missing in both *Pax3* and *Met* mutants (Prunotto et al., 2004;
457 Tajbakhsh et al., 1997; Tremblay et al., 1998). Therefore, the formation of the latissimus dorsi and
458 cutaneous maximus muscles depends on a specific developmental program implicating *Pax3*,
459 *Islet1* and *Met* genes. Given that the latissimus dorsi and cutaneous maximus participated in the
460 gain in mobility of the forelimbs towards the shoulder girdle in tetrapods, our findings provide
461 insights into their genetic and evolutionary origins.
462
463 Our detailed analysis of *Tbx1*- and *Pax3*-null mice on sections and in 3D reconstructions now
464 provides a clarified view of neck muscle morphogenesis (Table 2). In both *Tbx1* and *Pax3*
465 mutants, whereas the epaxial neck musculature is unaffected, the hypaxial muscles originating
466 from anterior somites are perturbed with a more severe phenotype observed in *Tbx1* mutants
467 (Table 2). Whereas no *Tbx1* expression has been reported in early myotomes in somites, *Tbx1*
468 transcripts appear in hypaxial limb and tongue precursors after myogenic specification (Grifone et
469 al., 2008; Kelly et al., 2004; Zoupa et al., 2006). *Tbx1*-null embryos show normal myotomal and

limb muscle morphology while the hypoglossal cord is hypoplastic, resulting in reduced tongue musculature (Table 2) (Grifone et al., 2008; Kelly et al., 2004). Therefore, we cannot exclude the possibility that *Tbx1* is activated and plays a role after specification of neck hypaxial muscles (Okano et al., 2008; Zoupa et al., 2006). The hypaxial muscle defects might also be secondary to a failure of caudal pharyngeal outgrowth (Kelly et al., 2004). While *Tbx1* acts cell autonomously in mesodermal progenitors (Kong et al., 2014; Zhang et al., 2006), its expression in pharyngeal endoderm might imply an indirect role in CPM myogenesis (Arnold et al., 2006). Defects in signalling from pharyngeal endoderm may explain the hypoglossal cord deficiency and the potential non-autonomous role for *Tbx1* in neck hypaxial myogenesis. Detailed analysis of muscle formation in conditional *Tbx1* mutants is needed to resolve the relative roles of *Tbx1* in neck myogenesis.

It has been shown that hypaxial muscles are perturbed to a greater extent than epaxial muscles in *Pax3* mutants (Tajbakhsh et al., 1997; Tremblay et al., 1998), suggesting a different requirement for *Pax3* in these muscle groups, possibly through differential gene regulation (Brown et al., 2005). An unexpected outcome of our analysis was that neck hypaxial muscles (derived from *Mesp1* and *Pax3* lineages) are less perturbed in *Pax3*-null mutants than hypaxial muscles deriving from more posterior somites (*Pax3* lineage only) (Table 2). These observations support our model that a distinct genetic program governs somitic neck muscles compared to more posterior trunk muscles.

Connectivity network of the neck and shoulders

Assessing the non-muscle contribution to the neck region is a major challenge due to the extensive participation of diverse cell types from different embryological origins. Previous studies in amphibians, chick and mouse reported that branchiomeric and hypobranchial connective tissue

originates from NCCs (Hanken and Gross, 2005; Kontges and Lumsden, 1996; Matsuoka et al., 2005; Noden, 1983; Olsson et al., 2001; Ziermann et al., 2018b). It has been shown that the neural crest provides connective tissue for muscles that link the head and shoulders, whereas mesodermal cells give rise to connective tissue for muscles connecting the trunk and limbs (Matsuoka et al., 2005).

Our findings demonstrate that not all branchiomeric muscles are composed of neural crest-derived connective tissue, thereby redefining a new limit for NCC contribution to the neck and shoulders. Unexpectedly, we noted that the contribution of the neural crest lineage is limited in infrahyoid and posterior branchiomeric muscles that connect skeletal components of mesodermal origin. Indeed, it appears that the connective tissue of muscles that link exclusively mesodermal skeletal derivatives is of mesodermal origin. In contrast, the connective tissue of cucullaris-derived muscles is of a mixed origin, first developing in a cranial NCC domain at early stages, then expanding to incorporate connective tissue from both neural crest and LPM populations (Figure 7B). While NCCs are present in the anterior trapezius, sternocleidomastoid and infrahyoid muscles, contribution decreases at posterior attachment sites. In parallel, the LPM gives rise to shoulder skeletal components and to connective tissue of associated musculature including trapezius muscles (Figure 7C). Therefore, the dual NCC/LPM origin of the trapezius connective tissue correlates with the embryonic origin of skeletal components to which it is connected.

Wnt1^{Cre} and *Sox10*^{Cre} NCC reporter mice were used to show that endochondral cells connecting the cucullaris-derived muscles on the scapula, clavicle and sternum share a common NCC origin with the connective tissue (Matsuoka et al., 2005). However, NCCs are not found in pectoral components of fish, axolotl and chick, while contribution to neurocranium is conserved, suggesting that NCC involvement in shoulder formation would be specific to mammals (Epperlein

et al., 2012; Kague et al., 2012; Piekarski et al., 2014; Ponomartsev et al., 2017). In contrast to this view, our lineage analysis reveals that the neural crest lineage shows limited contribution to cucullaris connective tissue and does not form endochondral cells at the posterior attachment sites (Figure 7C). Differences in genetic lineage tracers and reagents might explain these discordant results (Matsuoka et al., 2005). Taken together, our findings indicate that connective tissue composition in the neck region correlates with the cellular origin of the associated skeletal components, independently of the myogenic source or ossification mode (Figure 7D).

Evolutionary and clinical perspectives

Our findings demonstrate that the hybrid origin of the skeletal, connective tissue and muscle components of the neck is defined during early embryogenesis. The close proximity of neural crest, CPM, LPM and somitic populations is unique along the body plan and underscores the difficulty in defining their relative contributions to structures in the neck (Figure 7A-B). Our results refine the relative contributions of the neural crest and mesodermal derivatives in mouse, thereby providing a coherent view of embryonic components at the head-trunk interface in gnathostomes. Our study also highlights the mesodermal contribution to posterior branchiomeric and infrahyoid connections. This reinforces recent notions suggesting that the cranial NCCs and the postcranial rearrangement of mesodermal populations at the head-trunk interface had been central for the establishment of the neck during gnathostome evolution (Adachi et al., 2018; Kuratani et al., 2018; Lours-Calet et al., 2014; Nagashima et al., 2016; Sefton et al., 2016). The contribution of anterior mesoderm in the origin of the neck needs to be elucidated in future studies of gnathostomes.

Our study reveals that neck muscles develop in a complex domain that is distinct from the head and trunk (Figure 7A-D), and that might be a contributing factor to pathologies that affect subsets

of neck muscles in specific myopathies (Emery, 2002; Randolph and Pavlath, 2015). In human, *TBX1* has been identified as a major candidate gene for 22q11.2 deletion syndrome (Papangeli and Scambler, 2013). Laryngeal malformations, esophageal dysmotility and shortened neck are frequent in patients. Moreover, the neck deficiencies might not be exclusively due to cervical spine abnormalities but also to neck muscle defects (Hamidi et al., 2014; Leopold et al., 2012; Marom et al., 2012). Therefore, our analysis of *Tbx1*-null mutants provides a better understanding of the aetiology of the 22q11.2 deletion syndrome and has direct implications in establishing clinical diagnosis in cases where patients present failure in neck-associated functions.

MATERIALS AND METHODS

Animals

Animals were handled as per European Community guidelines and the ethics committee of the Institut Pasteur (CTEA) approved protocols. Males carrying the *Cre* driver gene, *Mef2c-AHF*^{Cre} (Verzi et al., 2005), *Islet1*^{Cre} (Srinivas et al., 2001), *Mesp1*^{Cre} (Saga et al., 1999), *Pax3*^{Cre} (Engleka et al., 2005), *Myf5*^{Cre} (Haldar et al., 2007), *Wnt1*^{Cre} (Danielian et al., 1998), *Prx1*^{Cre} (Logan et al., 2002), were crossed to reporter females from previously described lines including *Pax7*^{GPL} (Sambasivan et al., 2013), *Rosa26*$^{R\text{-}lacZ}$ (*R26R*) (Soriano, 1999), *R26*^{mTmG} (Muzumdar et al., 2007) and *R26*^{tdTomato} (Madisen et al., 2010). *Myf5*$^{nlacZ/+}$ KI mice and mice carrying the *Tbx1*^{tm1pa} allele (referred to as *Tbx1*-null) were previously described (Jerome and Papaioannou, 2001; Kelly et al., 2004; Tajbakhsh et al., 1996). To generate experimental *Pax3*-null foetuses, *Pax3*$^{WT/Cre}$ males and females were intercrossed (Engleka et al., 2005) (n=5 *Tbx1* and *Pax3* mutants analysed including n=2 by µCT scanning). Mice were crossed and maintained on a F1 C57/BL6:DBA2 background and genotyped by PCR. Mouse embryos and foetuses were collected between E9.5 and E18.5, with noon on the day of the vaginal plug considered as E0.5.

X-gal and immunofluorescence stainings

Whole-mount samples were analysed for beta-galactosidase activity with X-gal (0.6 mg/ml) in 1X PBS buffer (D1408, Sigma, St. Louis, MO) containing 4 mM potassium ferricyanide, 4 mM potassium ferrocyanide, 0.02% NP-40 and 2 mM $MgCl_2$ as previously described (Comai et al., 2014). For immunostaining on cryosections, foetuses were fixed 3h in 4% paraformaldehyde (PFA) (15710, Electron Microscopy Sciences, Hatfield, PA) 0.5 % Triton X-100 (T8787, Sigma) at 4°C, washed overnight at 4°C in PBS 0.1% Tween 20 (P1379, Sigma), cryopreserved in 30% sucrose in PBS and embedded in OCT for 12-16µm sectioning with a Leica cryostat (CM3050 S, Leica, Wetzlar, Germany). Cryosections were dried for 30 min and washed in PBS. For

579 immunostaining on paraffin sections, samples were fixed overnight in 4% PFA, dehydrated in
580 graded ethanol series and penetrated with Histoclear II (HS-202, National Diagnostics, Atlanta,
581 GA), embedded in paraffin and oriented in blocks. Paraffin blocks were sectioned at 10-12 µm
582 using a Leica microtome (Reichert-Jung 2035). Sections were then deparaffinized and rehydrated
583 by successive immersions in Histoclear, ethanol and PBS. Samples were then subjected to antigen
584 retrieval with 10 mM Citrate buffer (pH 6.0) using a 2100 Retriever (Aptum Biologics,
585 Rownhams, UK).
586
587 Rehydrated sections were blocked for 1h in 10% normal goat serum, 3% BSA, 0.5% Triton X-100
588 in PBS. Primary antibodies were diluted in blocking solution and incubated overnight at 4°C.
589 Primary antibodies included the following: β-gal (1/1000, chicken polyclonal, ab9361, Abcam,
590 Cambridge, UK; 1/750, rabbit polyclonal, MP 559761, MP Biomedicals, Illkirch, France), GFP
591 (1/500, chick polyclonal, 1020, Aves Labs, Tigard, OR; 1/1000, chick polyclonal, 13970, Abcam),
592 Islet1 (1/1000, mouse monoclonal IgG1, 40.2D6, DSHB), My32 (1/400, mouse monoclonal IgG1,
593 M4276, Sigma), Myod (1/100, mouse monoclonal IgG1, M3512, Dako, Santa Clara, CA), Pax7
594 (1/20, mouse monoclonal IgG1, AB_528428), Tcf4 (1/150, rabbit polyclonal, C48H11, Cell
595 Signalling, Leiden, Netherlands), Tnnt3 (1/200, monoclonal mouse IgG1, T6277, Sigma), Tomato
596 (1/500, rabbit polyclonal, 632496, Clontech, Shiga, Japan; 1/250, chick polyclonal, 600-901-379,
597 Rockland, Pottstown, PA) and Tuj1 (1/1000, monoclonal mouse IgG2a, BLE801202, Ozyme,
598 Montigny-le-Bretonneux, France). After 3 rounds of 15 min washes in PBS 0.1% Tween 20,
599 secondary antibodies were incubated in blocking solution 2h at RT together with 1µg/ml Hoechst
600 33342 to visualize nuclei. Secondary antibodies consisted of Alexa 488, 555 or 633 goat anti-
601 rabbit, anti-chicken or anti-mouse isotype specific (1/500, Jackson Immunoresearch,
602 Cambridgeshire, UK). After 3 rounds of 15 min washes in PBS 0.1% Tween 20, slides were
603 mounted in 70% glycerol for analysis.

For whole-mount immunofluorescence staining, embryos were dissected in PBS, fixed in 4% PFA, washed in PBS and stored at -20°C in 100% methanol. After rehydration in PBS, whole mount immunostainings were performed incubating the primary and secondary antibodies for 3 days each. Samples were cleared using benzyl alcohol/benzyl benzoate (BABB) clarification method (Yokomizo et al., 2012).

µCT scan analysis

For µCT scan analysis, the foetuses were treated with the phosphotungstic acid (PTA) contrast agent to well reveal skeletal and muscle structures. After dissection of the cervical region (including the mandible and scapular components, see Figure 2-figure supplement 1), the foetuses were fixed in 4% PFA for 24h at 4°C. Samples were then additionally fixed and dehydrated by exchanging the fixative and washing solutions to incrementally increasing ethanol concentrations (30%, 50%, 70%) with 2 days in each concentration to minimize the shrinkage of tissues. To start the contrasting procedure the embryos were firstly incubated in ethanol-methanol-water mixture (4:4:3) for 1h and then transferred for 1h into 80% and 90% methanol solution. The staining procedure was then performed for 10 days in 90% methanol 1.5% PTA solution (changed every day with fresh solution) to ensure optimal penetration of the contrast agent. Staining was followed by rehydration of the samples in methanol grade series (90%, 80%, 70%, 50% and 30%) and stored in sterile distilled water. The samples were placed in polypropylene tubes and embedded in 1% agarose gel to avoid movement artefacts during measurements. µCT scanning was performed using laboratory system GE Phoenix v|tome|x L 240 (GE Sensing & Inspection Technologies GmbH, Hamburg, Germany), equipped with a nanofocus X-ray tube with maximum power of 180 kV/15 W and a flat panel detector DXR250 with 2048 × 2048 pixel2, 200 × 200 μm^2 pixel size. The µCT scan was carried out at 60 kV acceleration voltage and 200 µA tube current with voxel

size of 5.7 µm for all samples. The beam was filtered by a 0.2 mm aluminium filter. The 2200 projections were taken over 360° with exposure time of 900 ms. The tomographic reconstructions were done using the software GE phoenix datos|x 2.0 (GE Sensing & Inspection Technologies GmbH) and data segmentations and visualizations were performed by combination of software VG Studio MAX 2.2 (Volume GraphicsGmbH, Heidelberg, Germany) and Avizo 7.1 (Thermo Fisher Scientific, Waltham, MA) according to (Tesařová et al., 2016). The interactive 3D PDFs were set up using 3D PDF maker software.

Imaging

Images were acquired using the following systems: a Zeiss Axio-plan equipped with an Apotome, a Zeiss stereo zoom microscope V16 or a Zeiss LSM 700 laser-scanning confocal microscope with ZEN software (Carl Zeiss, Oberkochen, Germany). For whole-mount rendering, acquired Z-stacks were 3D reconstructed using Imaris software. All images were assembled in Adobe Photoshop (Adobe Systems, San Jose, CA).

ACKNOWLEDGEMENTS

We thank Drs. Claudio Cortes and Françoise Helmbacher for providing transgenic mice and Mirialys Gallardo for technical assistance.

COMPETING INTERESTS

The authors declare no competing interests.

651 **REFERENCES**

652 Adachi, N., Pascual-Anaya, J., Hirai, T., Higuchi, S., Kuratani, S., 2018. Development of
653 hypobranchial muscles with special reference to the evolution of the vertebrate neck.
654 Zoological letters 4, 5.

655 Arnold, J.S., Werling, U., Braunstein, E.M., Liao, J., Nowotschin, S., Edelmann, W., Hebert, J.M.,
656 Morrow, B.E., 2006. Inactivation of Tbx1 in the pharyngeal endoderm results in 22q11DS
657 malformations. Development 133, 977-987.

658 Brown, C.B., Engleka, K.A., Wenning, J., Min Lu, M., Epstein, J.A., 2005. Identification of a
659 hypaxial somite enhancer element regulating Pax3 expression in migrating myoblasts and
660 characterization of hypaxial muscle Cre transgenic mice. Genesis 41, 202-209.

661 Burke, A.C., Nowicki, J.L., 2003. A new view of patterning domains in the vertebrate mesoderm.
662 Developmental cell 4, 159-165.

663 Cai, C.L., Liang, X., Shi, Y., Chu, P.H., Pfaff, S.L., Chen, J., Evans, S., 2003. Isl1 identifies a
664 cardiac progenitor population that proliferates prior to differentiation and contributes a majority
665 of cells to the heart. Developmental cell 5, 877-889.

666 Comai, G., Sambasivan, R., Gopalakrishnan, S., Tajbakhsh, S., 2014. Variations in the efficiency
667 of lineage marking and ablation confound distinctions between myogenic cell populations.
668 Developmental cell 31, 654-667.

669 Comai, G., Tajbakhsh, S., 2014. Molecular and cellular regulation of skeletal myogenesis. Current
670 topics in developmental biology 110, 1-73.

671 Couly, G.F., Coltey, P.M., Le Douarin, N.M., 1993. The triple origin of skull in higher
672 vertebrates: a study in quail-chick chimeras. Development 117, 409-429.

673 Danielian, P.S., Muccino, D., Rowitch, D.H., Michael, S.K., McMahon, A.P., 1998. Modification
674 of gene activity in mouse embryos in utero by a tamoxifen-inducible form of Cre recombinase.
675 Current biology : CB 8, 1323-1326.

676 Diogo, R., Kelly, R.G., Christiaen, L., Levine, M., Ziermann, J.M., Molnar, J.L., Noden, D.M.,
677 Tzahor, E., 2015. A new heart for a new head in vertebrate cardiopharyngeal evolution. Nature
678 520, 466-473.
679 Diogo, R.A., V. , 2010. Muscles of Vertebrates - Comparative Anatomy, Evolution, Homologies
680 and Development. Enfield, New Hampshire: Science Publishers.
681 Durland, J.L., Sferlazzo, M., Logan, M., Burke, A.C., 2008. Visualizing the lateral somitic frontier
682 in the Prx1Cre transgenic mouse. Journal of anatomy 212, 590-602.
683 Edgeworth, F.H., 1935. The cranial muscles of vertebrates. Cambridge University Press.
684 Emery, A.E., 2002. The muscular dystrophies. Lancet 359, 687-695.
685 Engleka, K.A., Gitler, A.D., Zhang, M., Zhou, D.D., High, F.A., Epstein, J.A., 2005. Insertion of
686 Cre into the Pax3 locus creates a new allele of Splotch and identifies unexpected Pax3
687 derivatives. Developmental biology 280, 396-406.
688 Epperlein, H.H., Khattak, S., Knapp, D., Tanaka, E.M., Malashichev, Y.B., 2012. Neural crest
689 does not contribute to the neck and shoulder in the axolotl (Ambystoma mexicanum). PloS one
690 7, e52244.
691 Ericsson, R., Knight, R., Johanson, Z., 2013. Evolution and development of the vertebrate neck.
692 Journal of anatomy 222, 67-78.
693 Evans, D.J., Noden, D.M., 2006. Spatial relations between avian craniofacial neural crest and
694 paraxial mesoderm cells. Developmental dynamics : an official publication of the American
695 Association of Anatomists 235, 1310-1325.
696 Gopalakrishnan, S., Comai, G., Sambasivan, R., Francou, A., Kelly, R.G., Tajbakhsh, S., 2015. A
697 Cranial Mesoderm Origin for Esophagus Striated Muscles. Developmental cell 34, 694-704.
698 Greil, A., 1913. Entwicklungsgeschichte des Kopfes und des Blutgefässsystemes von *Ceratodus*
699 *forsteri*. II. Die
700 epigenetischen Erwerbungen während der Stadien 39–48. Denkschr Med-Naturwiss Ges Jena.

701 Grifone, R., Jarry, T., Dandonneau, M., Grenier, J., Duprez, D., Kelly, R.G., 2008. Properties of
702 branchiomeric and somite-derived muscle development in Tbx1 mutant embryos.
703 Developmental dynamics : an official publication of the American Association of Anatomists
704 237, 3071-3078.
705 Haldar, M., Hancock, J.D., Coffin, C.M., Lessnick, S.L., Capecchi, M.R., 2007. A conditional
706 mouse model of synovial sarcoma: insights into a myogenic origin. Cancer cell 11, 375-388.
707 Hamidi, M., Nabi, S., Husein, M., Mohamed, M.E., Tay, K.Y., McKillop, S., 2014. Cervical spine
708 abnormalities in 22q11.2 deletion syndrome. Cleft Palate Craniofac J 51, 230-233.
709 Hanken, J., Gross, J.B., 2005. Evolution of cranial development and the role of neural crest:
710 insights from amphibians. Journal of anatomy 207, 437-446.
711 Haraguchi, S., Kitajima, S., Takagi, A., Takeda, H., Inoue, T., Saga, Y., 2001. Transcriptional
712 regulation of Mesp1 and Mesp2 genes: differential usage of enhancers during development.
713 Mechanisms of development 108, 59-69.
714 Harel, I., Nathan, E., Tirosh-Finkel, L., Zigdon, H., Guimaraes-Camboa, N., Evans, S.M., Tzahor,
715 E., 2009. Distinct origins and genetic programs of head muscle satellite cells. Developmental
716 cell 16, 822-832.
717 Huang, R., Zhi, Q., Ordahl, C.P., Christ, B., 1997. The fate of the first avian somite. Anatomy and
718 embryology 195, 435-449.
719 Huang, R., Zhi, Q., Patel, K., Wilting, J., Christ, B., 2000. Contribution of single somites to the
720 skeleton and muscles of the occipital and cervical regions in avian embryos. Anatomy and
721 embryology 202, 375-383.
722 Jerome, L.A., Papaioannou, V.E., 2001. DiGeorge syndrome phenotype in mice mutant for the T-
723 box gene, Tbx1. Nature genetics 27, 286-291.
724 Kague, E., Gallagher, M., Burke, S., Parsons, M., Franz-Odendaal, T., Fisher, S., 2012.
725 Skeletogenic fate of zebrafish cranial and trunk neural crest. PloS one 7, e47394.

726 Kassar-Duchossoy, L., Giacone, E., Gayraud-Morel, B., Jory, A., Gomes, D., Tajbakhsh, S., 2005.
727 Pax3/Pax7 mark a novel population of primitive myogenic cells during development. Genes &
728 development 19, 1426-1431.
729 Kelly, R.G., Jerome-Majewska, L.A., Papaioannou, V.E., 2004. The del22q11.2 candidate gene
730 Tbx1 regulates branchiomeric myogenesis. Human molecular genetics 13, 2829-2840.
731 Kong, P., Racedo, S.E., Macchiarulo, S., Hu, Z., Carpenter, C., Guo, T., Wang, T., Zheng, D.,
732 Morrow, B.E., 2014. Tbx1 is required autonomously for cell survival and fate in the pharyngeal
733 core mesoderm to form the muscles of mastication. Human molecular genetics 23, 4215-4231.
734 Kontges, G., Lumsden, A., 1996. Rhombencephalic neural crest segmentation is preserved
735 throughout craniofacial ontogeny. Development 122, 3229-3242.
736 Kuratani, S., 2008. Evolutionary developmental studies of cyclostomes and the origin of the
737 vertebrate neck. Development, growth & differentiation 50 Suppl 1, S189-194.
738 Kuratani, S., Kusakabe, R., Hirasawa, T., 2018. The neural crest and evolution of the head/trunk
739 interface in vertebrates. Developmental biology.
740 Leopold, C., De Barros, A., Cellier, C., Drouin-Garraud, V., Dehesdin, D., Marie, J.P., 2012.
741 Laryngeal abnormalities are frequent in the 22q11 deletion syndrome. Int J Pediatr
742 Otorhinolaryngol 76, 36-40.
743 Lescroart, F., Hamou, W., Francou, A., Theveniau-Ruissy, M., Kelly, R.G., Buckingham, M.,
744 2015. Clonal analysis reveals a common origin between nonsomite-derived neck muscles and
745 heart myocardium. Proceedings of the National Academy of Sciences of the United States of
746 America 112, 1446-1451.
747 Lescroart, F., Kelly, R.G., Le Garrec, J.F., Nicolas, J.F., Meilhac, S.M., Buckingham, M., 2010.
748 Clonal analysis reveals common lineage relationships between head muscles and second heart
749 field derivatives in the mouse embryo. Development 137, 3269-3279.

750 Loebel, D.A., Hor, A.C., Bildsoe, H., Jones, V., Chen, Y.T., Behringer, R.R., Tam, P.P., 2012.
751 Regionalized Twist1 activity in the forelimb bud drives the morphogenesis of the proximal and
752 preaxial skeleton. Developmental biology 362, 132-140.
753 Logan, M., Martin, J.F., Nagy, A., Lobe, C., Olson, E.N., Tabin, C.J., 2002. Expression of Cre
754 Recombinase in the developing mouse limb bud driven by a Prxl enhancer. Genesis 33, 77-80.
755 Lours-Calet, C., Alvares, L.E., El-Hanfy, A.S., Gandesha, S., Walters, E.H., Sobreira, D.R.,
756 Wotton, K.R., Jorge, E.C., Lawson, J.A., Kelsey Lewis, A., Tada, M., Sharpe, C., Kardon, G.,
757 Dietrich, S., 2014. Evolutionarily conserved morphogenetic movements at the vertebrate head-
758 trunk interface coordinate the transport and assembly of hypopharyngeal structures.
759 Developmental biology 390, 231-246.
760 Lubosch, W., 1938. Muskeln des Kopfes: Viscerale Muskulatur. In: Bolk L, Göppert E, Kallius E,
761 Lubosch W Handbuch Der Vergleichenden Anatomie Der Wirbeltiere. Berlin: Urban &
762 Schwarzenberg.
763 Madisen, L., Zwingman, T.A., Sunkin, S.M., Oh, S.W., Zariwala, H.A., Gu, H., Ng, L.L.,
764 Palmiter, R.D., Hawrylycz, M.J., Jones, A.R., Lein, E.S., Zeng, H., 2010. A robust and high-
765 throughput Cre reporting and characterization system for the whole mouse brain. Nature
766 neuroscience 13, 133-140.
767 Marom, T., Roth, Y., Goldfarb, A., Cinamon, U., 2012. Head and neck manifestations of 22q11.2
768 deletion syndromes. Eur Arch Otorhinolaryngol 269, 381-387.
769 Martin, A.R., Reddy, R., Fehlings, M.G., 2011. Dropped head syndrome: diagnosis and
770 management. Evidence-based spine-care journal 2, 41-47.
771 Matsuoka, T., Ahlberg, P.E., Kessaris, N., Iannarelli, P., Dennehy, U., Richardson, W.D.,
772 McMahon, A.P., Koentges, G., 2005. Neural crest origins of the neck and shoulder. Nature 436,
773 347-355.

774 McGonnell, I.M., McKay, I.J., Graham, A., 2001. A population of caudally migrating cranial
775 neural crest cells: functional and evolutionary implications. Developmental biology 236, 354-
776 363.
777 Moreno, T.A., Jappelli, R., Izpisua Belmonte, J.C., Kintner, C., 2008. Retinoic acid regulation of
778 the Mesp-Ripply feedback loop during vertebrate segmental patterning. Developmental biology
779 315, 317-330.
780 Muzumdar, M.D., Tasic, B., Miyamichi, K., Li, L., Luo, L., 2007. A global double-fluorescent
781 Cre reporter mouse. Genesis 45, 593-605.
782 Nagashima, H., Sugahara, F., Watanabe, K., Shibata, M., Chiba, A., Sato, N., 2016.
783 Developmental origin of the clavicle, and its implications for the evolution of the neck and the
784 paired appendages in vertebrates. Journal of anatomy 229, 536-548.
785 Nassari, S., Duprez, D., Fournier-Thibault, C., 2017. Non-myogenic Contribution to Muscle
786 Development and Homeostasis: The Role of Connective Tissues. Frontiers in cell and
787 developmental biology 5, 22.
788 Nathan, E., Monovich, A., Tirosh-Finkel, L., Harrelson, Z., Rousso, T., Rinon, A., Harel, I.,
789 Evans, S.M., Tzahor, E., 2008. The contribution of Islet1-expressing splanchnic mesoderm
790 cells to distinct branchiomeric muscles reveals significant heterogeneity in head muscle
791 development. Development 135, 647-657.
792 Naumann, B., Warth, P., Olsson, L., Konstantinidis, P., 2017. The development of the cucullaris
793 muscle and the branchial musculature in the Longnose Gar, (Lepisosteus osseus,
794 Lepisosteiformes, Actinopterygii) and its implications for the evolution and development of the
795 head/trunk interface in vertebrates. Evolution & development 19, 263-276.
796 Noda, M., Miyake, T., Okabe, M., 2017. Development of cranial muscles in the actinopterygian
797 fish Senegal bichir, Polypterus senegalus Cuvier, 1829. J Morphol 278, 450-463.

798 Noden, D.M., 1983. The embryonic origins of avian cephalic and cervical muscles and associated
799 connective tissues. The American journal of anatomy 168, 257-276.
800 Noden, D.M., 1988. Interactions and fates of avian craniofacial mesenchyme. Development 103
801 Suppl, 121-140.
802 Noden, D.M., Francis-West, P., 2006. The differentiation and morphogenesis of craniofacial
803 muscles. Developmental dynamics : an official publication of the American Association of
804 Anatomists 235, 1194-1218.
805 Okano, J., Sakai, Y., Shiota, K., 2008. Retinoic acid down-regulates Tbx1 expression and induces
806 abnormal differentiation of tongue muscles in fetal mice. Developmental dynamics : an official
807 publication of the American Association of Anatomists 237, 3059-3070.
808 Olsson, L., Falck, P., Lopez, K., Cobb, J., Hanken, J., 2001. Cranial neural crest cells contribute to
809 connective tissue in cranial muscles in the anuran amphibian, Bombina orientalis.
810 Developmental biology 237, 354-367.
811 Papangeli, I., Scambler, P., 2013. The 22q11 deletion: DiGeorge and velocardiofacial syndromes
812 and the role of TBX1. Wiley interdisciplinary reviews. Developmental biology 2, 393-403.
813 Piatt, J., 1938. Morphogenesis of the cranial muscles of *Amblystoma punctatum*. Journal of
814 Morphology 63, 531-587.
815 Piekarski, N., Gross, J.B., Hanken, J., 2014. Evolutionary innovation and conservation in the
816 embryonic derivation of the vertebrate skull. Nat Commun 5, 5661.
817 Piekarski, N., Olsson, L., 2007. Muscular derivatives of the cranialmost somites revealed by long-
818 term fate mapping in the Mexican axolotl (Ambystoma mexicanum). Evolution & development
819 9, 566-578.
820 Ponomartsev, S., Valasek, P., Patel, K., Malashichev, Y.B., 2017. Neural crest contribution to the
821 avian shoulder girdle and implications to girdle evolution in vertebrates. Biological
822 Communications 62, 26-37.

823 Prunotto, C., Crepaldi, T., Forni, P.E., Ieraci, A., Kelly, R.G., Tajbakhsh, S., Buckingham, M.,
824 Ponzetto, C., 2004. Analysis of Mlc-lacZ Met mutants highlights the essential function of Met
825 for migratory precursors of hypaxial muscles and reveals a role for Met in the development of
826 hyoid arch-derived facial muscles. Developmental dynamics : an official publication of the
827 American Association of Anatomists 231, 582-591.
828 Randolph, M.E., Pavlath, G.K., 2015. A muscle stem cell for every muscle: variability of satellite
829 cell biology among different muscle groups. Frontiers in aging neuroscience 7, 190.
830 Relaix, F., Rocancourt, D., Mansouri, A., Buckingham, M., 2004. Divergent functions of murine
831 Pax3 and Pax7 in limb muscle development. Genes & development 18, 1088-1105.
832 Relaix, F., Rocancourt, D., Mansouri, A., Buckingham, M., 2005. A Pax3/Pax7-dependent
833 population of skeletal muscle progenitor cells. Nature 435, 948-953.
834 Saga, Y., 1998. Genetic rescue of segmentation defect in MesP2-deficient mice by MesP1 gene
835 replacement. Mechanisms of development 75, 53-66.
836 Saga, Y., Hata, N., Kobayashi, S., Magnuson, T., Seldin, M.F., Taketo, M.M., 1996. MesP1: a
837 novel basic helix-loop-helix protein expressed in the nascent mesodermal cells during mouse
838 gastrulation. Development 122, 2769-2778.
839 Saga, Y., Kitajima, S., Miyagawa-Tomita, S., 2000. Mesp1 expression is the earliest sign of
840 cardiovascular development. Trends in cardiovascular medicine 10, 345-352.
841 Saga, Y., Miyagawa-Tomita, S., Takagi, A., Kitajima, S., Miyazaki, J., Inoue, T., 1999. MesP1 is
842 expressed in the heart precursor cells and required for the formation of a single heart tube.
843 Development 126, 3437-3447.
844 Sambasivan, R., Comai, G., Le Roux, I., Gomes, D., Konge, J., Dumas, G., Cimper, C.,
845 Tajbakhsh, S., 2013. Embryonic founders of adult muscle stem cells are primed by the
846 determination gene Mrf4. Developmental biology 381, 241-255.

847 Sambasivan, R., Gayraud-Morel, B., Dumas, G., Cimper, C., Paisant, S., Kelly, R.G., Tajbakhsh,
848 S., 2009. Distinct regulatory cascades govern extraocular and pharyngeal arch muscle
849 progenitor cell fates. Developmental cell 16, 810-821.
850 Satou, Y., Imai, K.S., Satoh, N., 2004. The ascidian Mesp gene specifies heart precursor cells.
851 Development 131, 2533-2541.
852 Sawada, A., Fritz, A., Jiang, Y.J., Yamamoto, A., Yamasu, K., Kuroiwa, A., Saga, Y., Takeda, H.,
853 2000. Zebrafish Mesp family genes, mesp-a and mesp-b are segmentally expressed in the
854 presomitic mesoderm, and Mesp-b confers the anterior identity to the developing somites.
855 Development 127, 1691-1702.
856 Sefton, E.M., Bhullar, B.A., Mohaddes, Z., Hanken, J., 2016. Evolution of the head-trunk
857 interface in tetrapod vertebrates. eLife 5, e09972.
858 Soriano, P., 1999. Generalized lacZ expression with the ROSA26 Cre reporter strain. Nature
859 genetics 21, 70-71.
860 Srinivas, S., Watanabe, T., Lin, C.S., William, C.M., Tanabe, Y., Jessell, T.M., Costantini, F.,
861 2001. Cre reporter strains produced by targeted insertion of EYFP and ECFP into the ROSA26
862 locus. BMC developmental biology 1, 4.
863 Tabler, J.M., Rigney, M.M., Berman, G.J., Gopalakrishnan, S., Heude, E., Al-Lami, H.A.,
864 Yannakoudakis, B.Z., Fitch, R.D., Carter, C., Vokes, S., Liu, K.J., Tajbakhsh, S., Egnor, S.R.,
865 Wallingford, J.B., 2017. Cilia-mediated Hedgehog signaling controls form and function in the
866 mammalian larynx. eLife 6.
867 Tada, M.N., Kuratani, S., 2015. Evolutionary and developmental understanding of the spinal
868 accessory nerve. Zoological letters 1, 4.
869 Tajbakhsh, S., Rocancourt, D., Buckingham, M., 1996. Muscle progenitor cells failing to respond
870 to positional cues adopt non-myogenic fates in myf-5 null mice. Nature 384, 266-270.

871 Tajbakhsh, S., Rocancourt, D., Cossu, G., Buckingham, M., 1997. Redefining the genetic
872 hierarchies controlling skeletal myogenesis: Pax-3 and Myf-5 act upstream of MyoD. Cell 89,
873 127-138.
874 Tesařová, M., Zikmund, T., Kaucká, M., Adameyko, I., Jaroš, J., Paloušek, D., Škaroupka, D.,
875 Kaiser, J., 2016. Use of micro computed-tomography and 3D printing for reverse engineering
876 of mouse embryo nasal capsule. Journal of Instrumentation 11.
877 Theis, S., Patel, K., Valasek, P., Otto, A., Pu, Q., Harel, I., Tzahor, E., Tajbakhsh, S., Christ, B.,
878 Huang, R., 2010. The occipital lateral plate mesoderm is a novel source for vertebrate neck
879 musculature. Development 137, 2961-2971.
880 Tremblay, P., Dietrich, S., Mericskay, M., Schubert, F.R., Li, Z., Paulin, D., 1998. A crucial role
881 for Pax3 in the development of the hypaxial musculature and the long-range migration of
882 muscle precursors. Developmental biology 203, 49-61.
883 Valasek, P., Theis, S., Krejci, E., Grim, M., Maina, F., Shwartz, Y., Otto, A., Huang, R., Patel, K.,
884 2010. Somitic origin of the medial border of the mammalian scapula and its homology to the
885 avian scapula blade. Journal of anatomy 216, 482-488.
886 Verzi, M.P., McCulley, D.J., De Val, S., Dodou, E., Black, B.L., 2005. The right ventricle,
887 outflow tract, and ventricular septum comprise a restricted expression domain within the
888 secondary/anterior heart field. Developmental biology 287, 134-145.
889 Yabe, T., Hoshijima, K., Yamamoto, T., Takada, S., 2016. Quadruple zebrafish mutant reveals
890 different roles of Mesp genes in somite segmentation between mouse and zebrafish.
891 Development 143, 2842-2852.
892 Yang, L., Cai, C.L., Lin, L., Qyang, Y., Chung, C., Monteiro, R.M., Mummery, C.L., Fishman,
893 G.I., Cogen, A., Evans, S., 2006. Isl1Cre reveals a common Bmp pathway in heart and limb
894 development. Development 133, 1575-1585.

895 Yokomizo, T., Yamada-Inagawa, T., Yzaguirre, A.D., Chen, M.J., Speck, N.A., Dzierzak, E.,
896 2012. Whole-mount three-dimensional imaging of internally localized immunostained cells
897 within mouse embryos. Nature protocols 7, 421-431.
898 Zhang, Z., Huynh, T., Baldini, A., 2006. Mesodermal expression of Tbx1 is necessary and
899 sufficient for pharyngeal arch and cardiac outflow tract development. Development 133, 3587-
900 3595.
901 Ziermann, J.M., Clement, A.M., Ericsson, R., Olsson, L., 2018a. Cephalic muscle development in
902 the Australian lungfish, Neoceratodus forsteri. J Morphol 279, 494-516.
903 Ziermann, J.M., Diogo, R., Noden, D.M., 2018b. Neural crest and the patterning of vertebrate
904 craniofacial muscles. Genesis, e23097.
905 Ziermann, J.M., Freitas, R., Diogo, R., 2017. Muscle development in the shark Scyliorhinus
906 canicula: implications for the evolution of the gnathostome head and paired appendage
907 musculature. Frontiers in zoology 14, 31.
908 Zoupa, M., Seppala, M., Mitsiadis, T., Cobourne, M.T., 2006. Tbx1 is expressed at multiple sites
909 of epithelial-mesenchymal interaction during early development of the facial complex. The
910 International journal of developmental biology 50, 504-510.
911
913

FIGURE LEGENDS

Figure 1. Genetic lineage tracing of neck muscle progenitors.

Whole-mount X-gal stainings of *Mef2c-AHF^{Cre};R26R*, *Islet1^{Cre};Pax7^{GPL}*, *Mesp1^{Cre};Pax7^{GPL}* and *Pax3^{Cre};Pax7^{GPL}* mice at E10.5 (A-D), E11.75 (E-H) and E18.5 (I-L') (n=3 for each condition). See associated figure supplements 1-2.

(A-H) Note labelling of mesodermal core of pharyngeal arches (PAs) and cucullaris anlage (*ccl*) by *Mef2c-AHF*, *Islet1* and *Mesp1* lineage reporters; β-gal+ cells in anterior somites of *Mesp1^{Cre}* embryos and in the *clp* anlagen of *Islet1^{Cre}* embryos. *Pax3* lineage marked somitic mesoderm.

(I-L') *Mef2c-AHF*, *Islet1* and *Mesp1* lineages marked branchiomeric (mas, trp, dg) and cucullaris muscles (stm, atp and stp). *Pax3^{Cre}* and *Mesp1^{Cre}* labelled somitic epaxial neck muscles.

atp, acromiotrapezius; ccl, cucullaris anlage; clp, cutaneous maximus/latissimus dorsi precursor; dg, digastric h, heart; hc, hypoglossal cord; lbm, limb muscle anlagen and limb muscles; ltd, latissimus dorsi; mas, masseter; nc, nasal capsule; nt, neural tube; PA1-2, pharyngeal arches 1-2; S3, somite 3; stm, sternocleidomastoid; stp, spinotrapezius; trp; temporal. Scale bars: in D for A-D and in H for E-H, 1000 µm; in L for I-L', 2000 µm.

Figure 2. Differential contributions of *Mesp1* and *Pax3* lineages to neck and shoulders.

Immunostainings on coronal cryosections of E18.5 *Mesp1^{Cre};R26^{tdTomato}* and *Pax3^{Cre};R26^{tdTomato}* mice for the myofibre Tnnt3 and Tomato markers at levels indicated in Figure 1. Higher magnifications of selected areas in (A-J) are shown in figure supplement 2; (n=2 for each condition). See also figure supplement 1.

(A-H) *Mesp1^{Cre}* labelled all neck muscles including branchiomeric (myh, esm, phm and ilm), cucullaris (stm, atp), somitic epaxial (epm) and hypaxial (tg, lcp, lcl, ifh) muscles. *Pax3^{Cre}* marked somitic muscles.

(I-J) At shoulder level, *Mesp1*-derived cells did not contribute to posterior somitic myofibres including scapular muscles (scm) compared to that observed in *Pax3*^{Cre} embryos.

ac, arytenoid cartilage; acp, scapular acromion process; atp, acromiotrapezius; cc, cricoid cartilage; esm, esophagus striated muscle; ifh, infrahyoid muscles; ilm, intrinsic laryngeal muscles; lcl, longus colli; lcp, longus capitis; myh, mylohyoid; ob, occipital bone; oc, otic capsule; phm, pharyngeal muscles; stm, sternocleidomastoid; scm, scapular musculature; tc, thyroid cartilage; tg, tongue muscles. Scale bars: in J for A-B 200 µm, for C-J 400 µm.

Figure 3. Neural crest contribution to neck muscle-associated tissue.

Immunostainings on coronal cryosections of E18.5 *Wnt1*^{Cre}*;R26*^{tdTomato} mice at levels indicated in Figure 1. Tnnt3/Tomato immunostainings are shown in (A-D) and immunostainings for Tuj1/Tomato on selected areas of (A-D) are shown with higher magnifications in (A'-D'). See associated figure supplements 1-4; (n=2).

(A-A') Note high *Wnt1* contribution in the acromiotrapezius but not epaxial muscles where *Wnt1*-derived cells marked neuronal cells.

(B-C') *Wnt1*-derived cells marked differentially the distinct muscles composing the sternocleidomastoid and laryngeal musculatures.

(D-D') At shoulder level, the *Wnt1* cells did not contribute to attachment of acromiotrapezius to scapula.

ac, arytenoid cartilage; acp, scapular acromion process; atp, acromiotrapezius; cc, cricoid cartilage; clm, cleidomastoid; clo, cleido-occipitalis; ct, cricothyroid; ifh, infrahyoid muscles; lca, lateral cricoarytenoid; MCT, muscle-associated connective tissue; phm, pharyngeal muscles; std, sternomastoid; tam, thyroarytenoid muscle; tc, thyroid cartilage. Scale bars: in D' for A-D 400 µm for A'-D' 200 µm.

964 **Figure 4. *Prx1*-LPM lineage contribution to neck and pectoral girdle.**

965 See also Figure supplements 1-2.

966 (A-D) X-gal stainings of *Prx1*^{Cre}*;R26R* reporter mice at E9.5 (n=3) (A) and E18.5 (n=3) (C-D),

967 and immunostaining for GFP and the Pax7/Myod/My32 myogenic markers in *Prx1*^{Cre}*;R26*^{mTmG}

968 E12.5 embryo (n=2) (B). Note *Prx1*-derived cells in postcranial LPM (A, black arrowheads) and

969 *Prx1*-derived cells among, but not in, cucullaris myofibres (B-D).

970 (E-F'') Immunostaining for β-gal, Tnnt3 and Tcf4 on coronal cryosections of E18.5 *Prx1*^{Cre}*;R26R*

971 mice (n=2) showed β-gal+ cells constituting the pectoral girdle (E, level C in Figure 1) and in

972 MCT fibroblasts (F-F'', white arrowheads), but not in trapezius myofibres.

973 acp, scapular acromion process; atp, acromiotrapezius; ccl, cucullaris anlage; ccp, scapular

974 coracoid process; cl, clavicle; epm, epaxial neck musculature; hh, humeral head; LPM, lateral

975 plate mesoderm; lb, forelimb bud; lbm, limb muscle anlagen; ltd, latissimus dorsi; PA1-6,

976 pharyngeal arches 1-6; S3, somite 3; scm, scapular muscles; stm, sternocleidomastoid; stp,

977 spinotrapezius. Scale bars: in A for A, B 500 µm; in C for C-D 2000 µm, for E 500 µm; in F'' for

978 F-F'' 20µm.

979

980 **Figure 5. Neck muscle phenotypes in *Tbx1* and *Pax3* mutants.**

981 Immunostainings for Tnnt3 differentiation marker on coronal cryosections of control, *Tbx1-null*

982 and *Pax3-null* foetuses at E18.5 (n=3 each condition). Yellow asterisks indicate missing muscles.

983 (A-I) Note absence of branchiomeric laryngeal, esophagus and trapezius muscles and severe

984 alteration of somitic hypaxial muscles in *Tbx1* mutants. Scapular and pectoral muscles are missing

985 in *Pax3* mutants.

986 ac, arytenoid cartilage; atp, acromiotrapezius; cc, cricoid cartilage; cl, clavicle; esm, esophagus

987 striated muscle; ifh, infrahyoid muscles; ilm, intrinsic laryngeal muscles; lcp, longus capitis; ptm,

pectoralis muscles; sc, scapula; st, sternum; tc, thyroid cartilage; tg, tongue musculature. Scale bars: in A for A-I 500 µm.

Figure 6. 3D reconstructions of neck musculoskeletal system in *Tbx1* and *Pax3* mutants.

See interactive 3D PDFs in Rich Media Files 1-3; control n=1; mutants n=2.

(A-C) Branchiomeric and cucullaris muscles marked by *Mef2c-AHF/Islet1/Mesp1* are indicated in pink.

(D-F) anterior somitic muscles (*Mesp1*, *Pax3* lineages), in red.

(G-I) scapular muscles from more posterior somites (*Pax3* lineage), in violet.

atp, acromiotrapezius; dg, digastric muscles; epm, epaxial neck musculature; ifh, infrahyoid muscles; ilm, intrinsic laryngeal muscles; lcl, longus colli; lcp, longus capitis; myh, mylohyoid; sc, scapula; scm, scapular muscles; stm, sternocleidomastoid; tc, thyroid cartilage; tg, tongue musculature.

Figure 7. Model for musculoskeletal and connective tissue relationships during murine neck development.

(A, C) CPM (pink), anterior somites (red) and more posterior somites (violet) –derived muscles are defined by three distinct genetic programs. Note that the cucullaris develops a in NC domain (blue), but is excluded from the postcranial LPM (yellow) (B). Dual NC/LPM origin of trapezius connective tissue is indicated (C-a). NC contribution to connective tissue extends to tongue and anterior infrahyoid musculature (C-b).

(D) Mixed origins of muscle connective tissues at the head-trunk-limb interface.

atp, acromiotrapezius; ccl, cucullaris; CPM, cardiopharyngeal mesoderm; epm, epaxial neck muscles; hpm, hypaxial neck muscles; LPM, postcranial lateral plate mesoderm; NC, neural crest;

1012 PA1-2, pharyngeal arches 1-2; PM, paraxial mesoderm; stm, sternocleidomastoid; stp,

1013 spinotrapezius.

1014

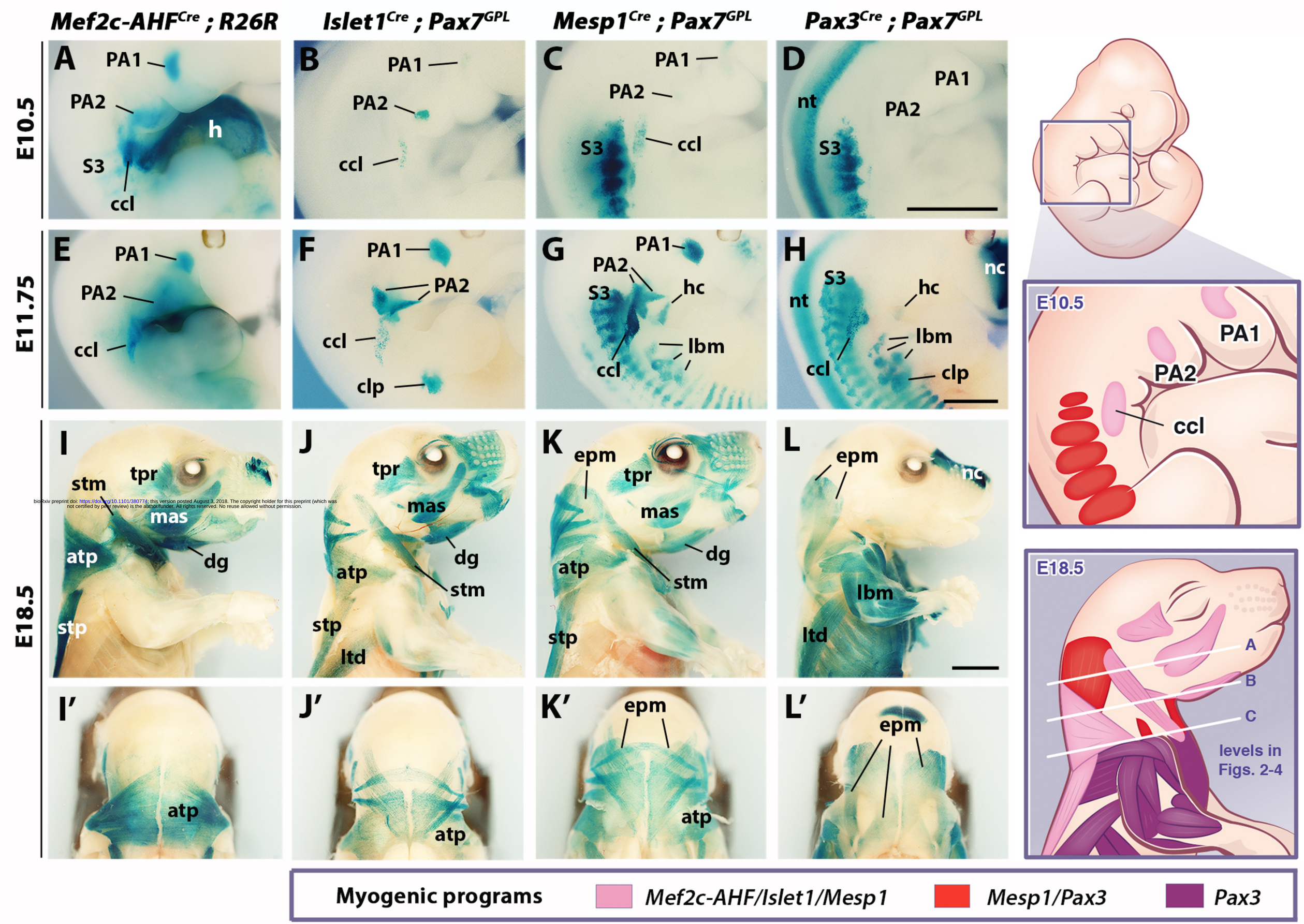

Figure 1

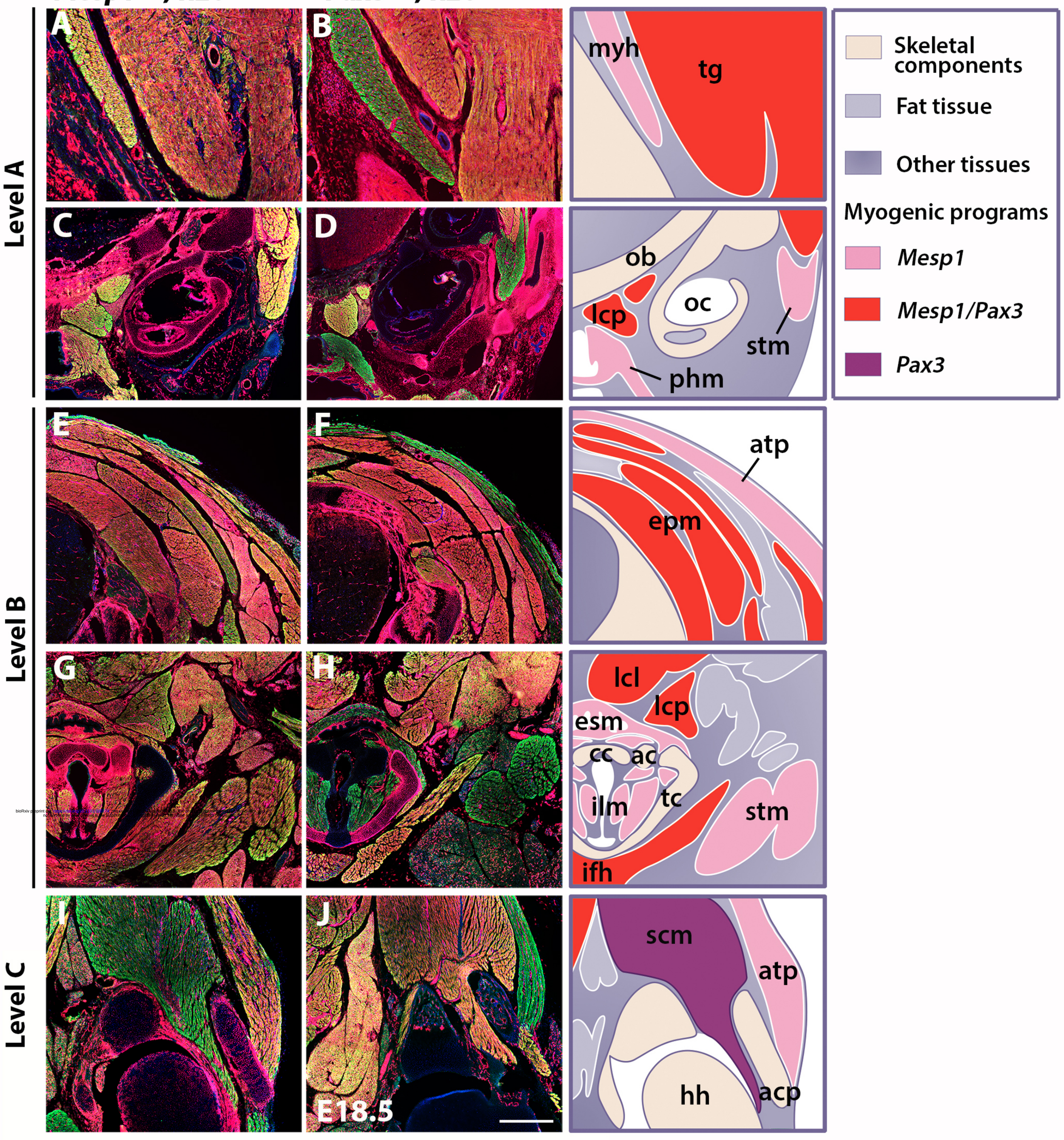

Figure 2

Wnt1^{Cre}; R26^{tdTomato}

Level B

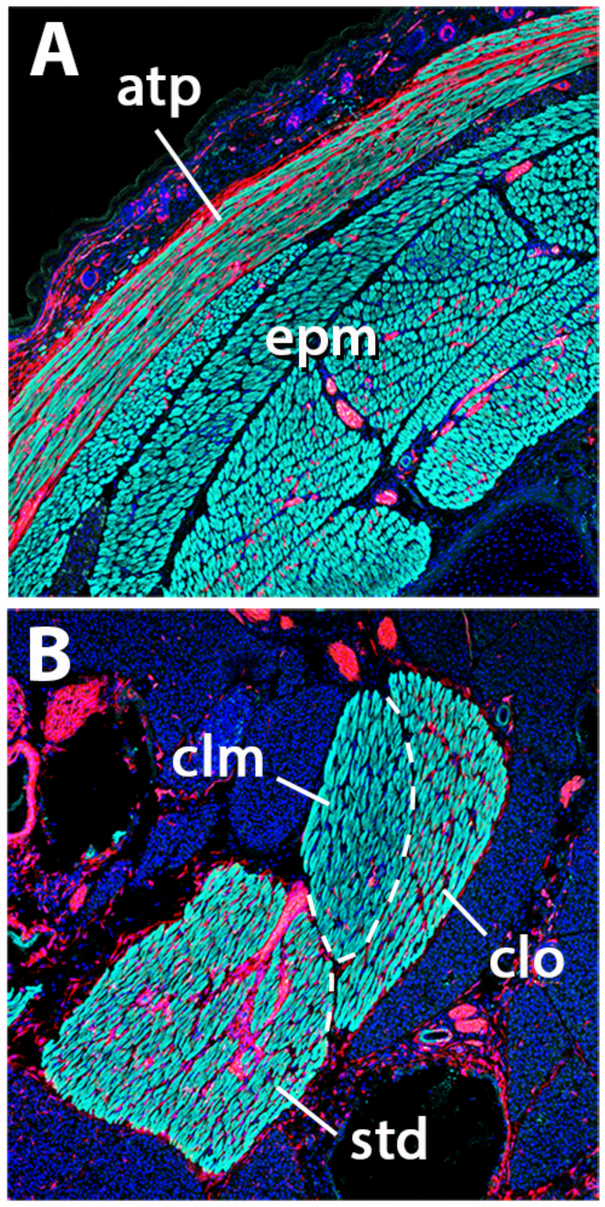

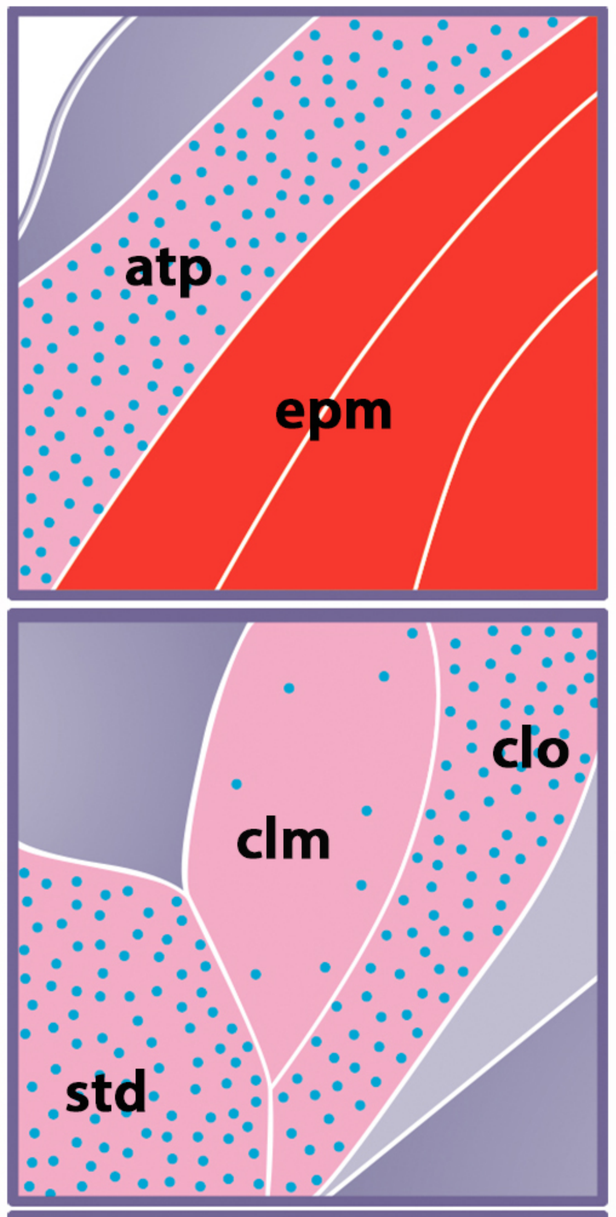

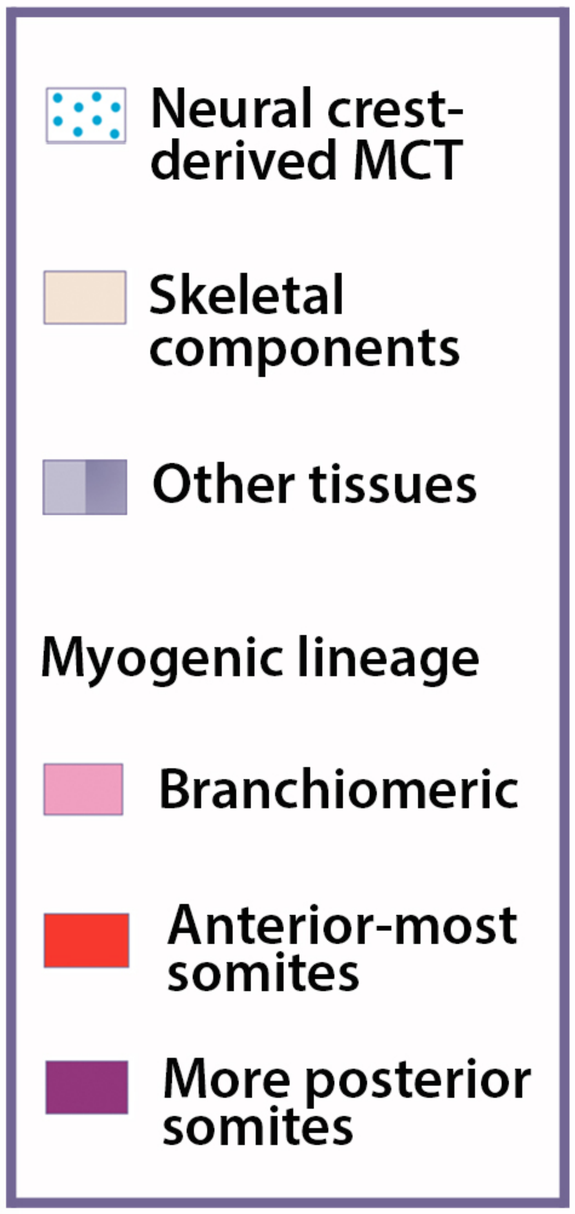

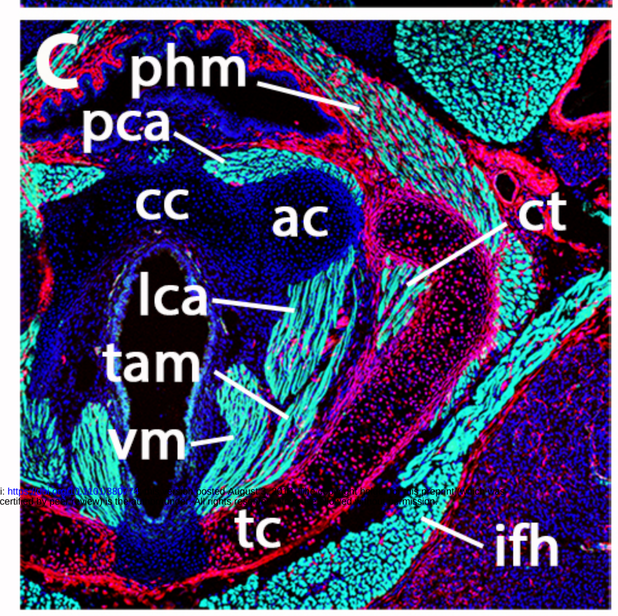

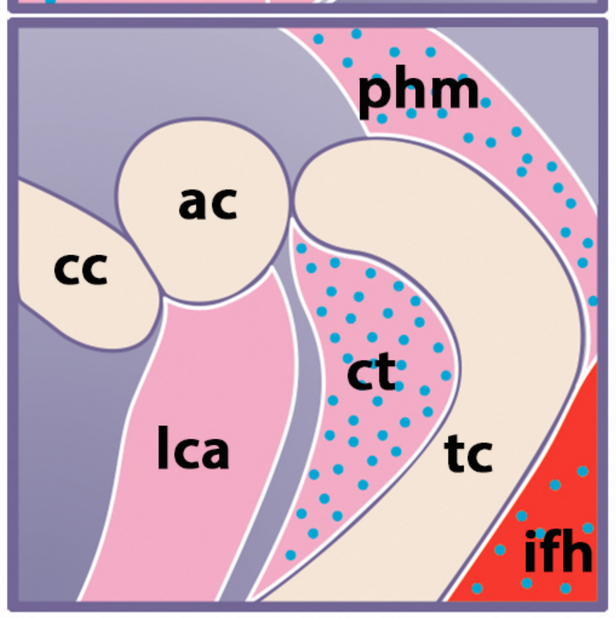

Level C

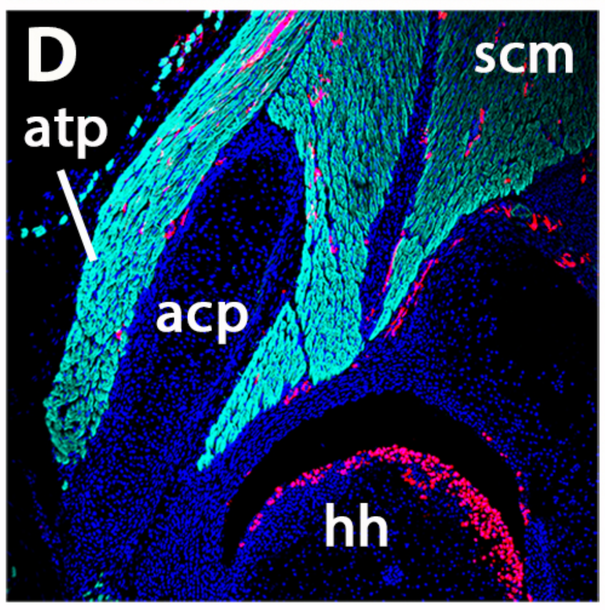

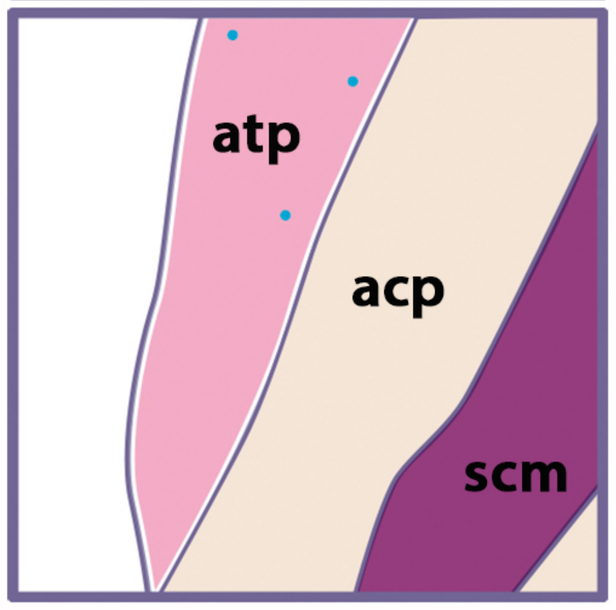

Hoechst Tnnt3 Tomato Hoechst Tuj1 Tomato

Figure 3

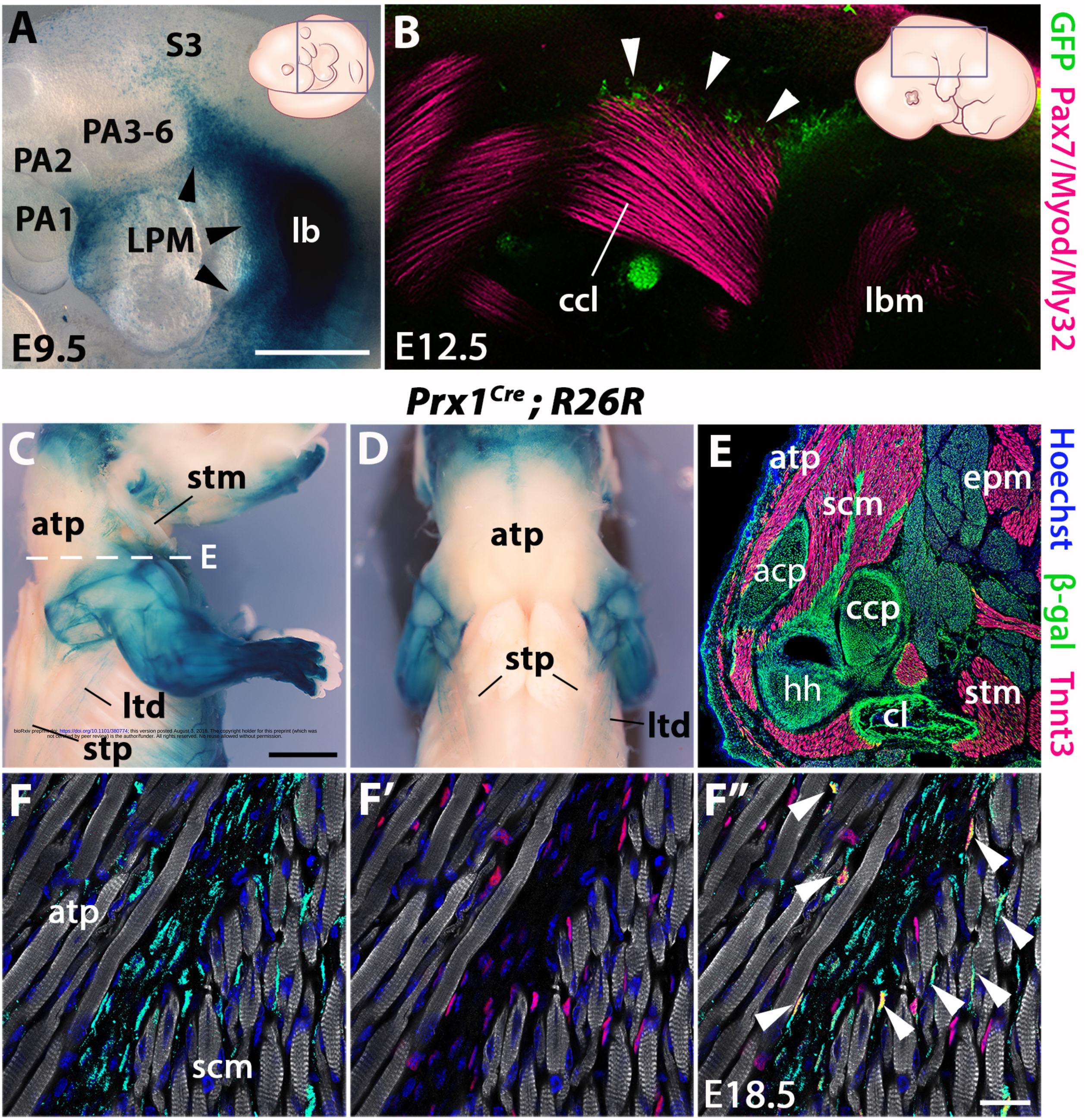

Figure 4

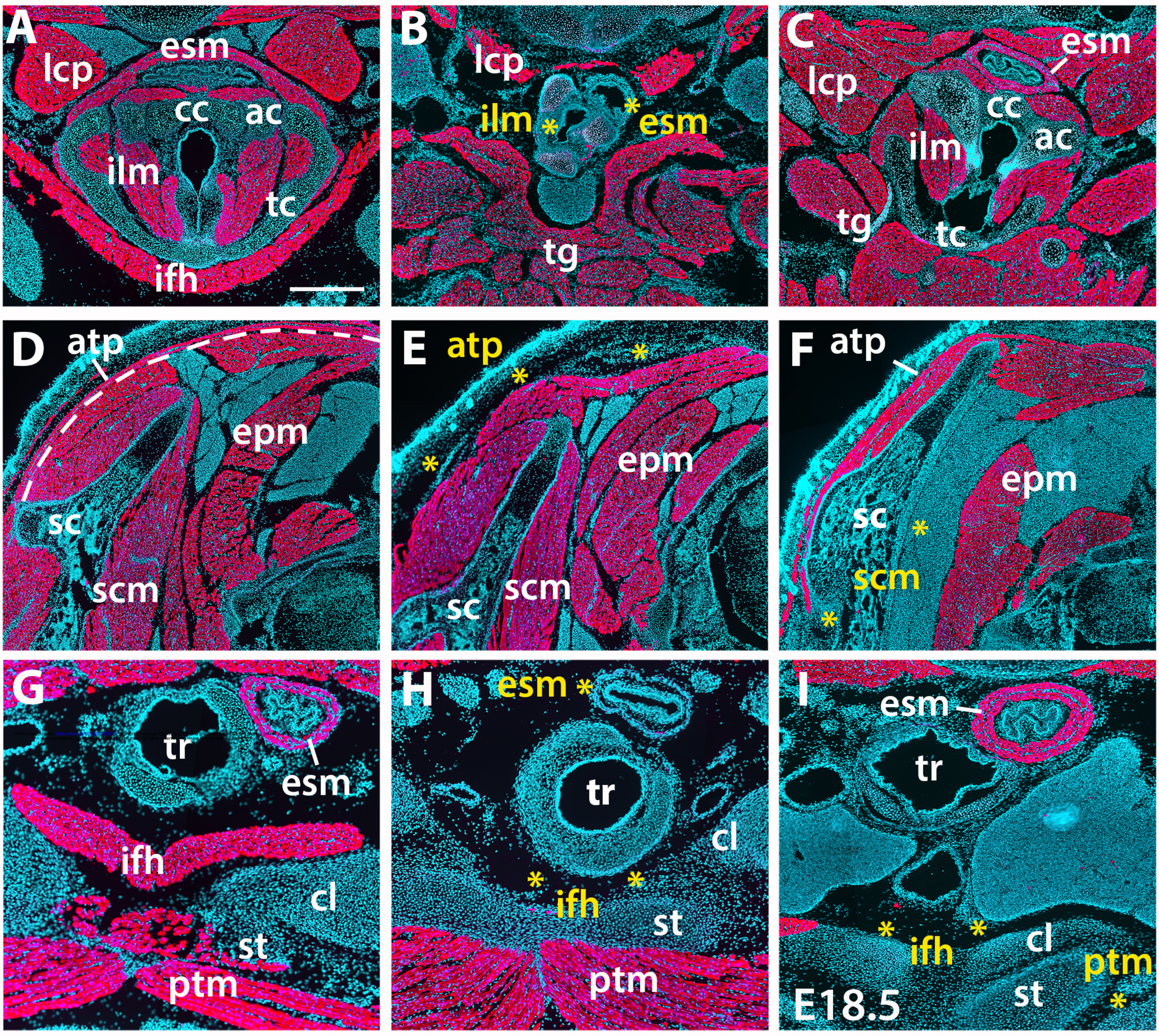
Ctrl
Tbx1-/-
Pax3-/-
A
lcp
esm
cc
ac
ilm
tc
ifh
B
lcp
ilm
esm
tg
C
esm
lcp
cc
ac
ilm
tg
tc
D
atp
epm
sc
scm
E
atp
epm
sc
scm
F
atp
epm
sc
scm
G
tr
esm
ifh
cl
st
ptm
H
esm
tr
cl
ifh
st
ptm
I
esm
tr
ifh
cl
ptm
st
E18.5
Hoechst Tnnt3

Figure 5

Ctrl

Tbx1$^{-/-}$

Pax3$^{-/-}$

ventral

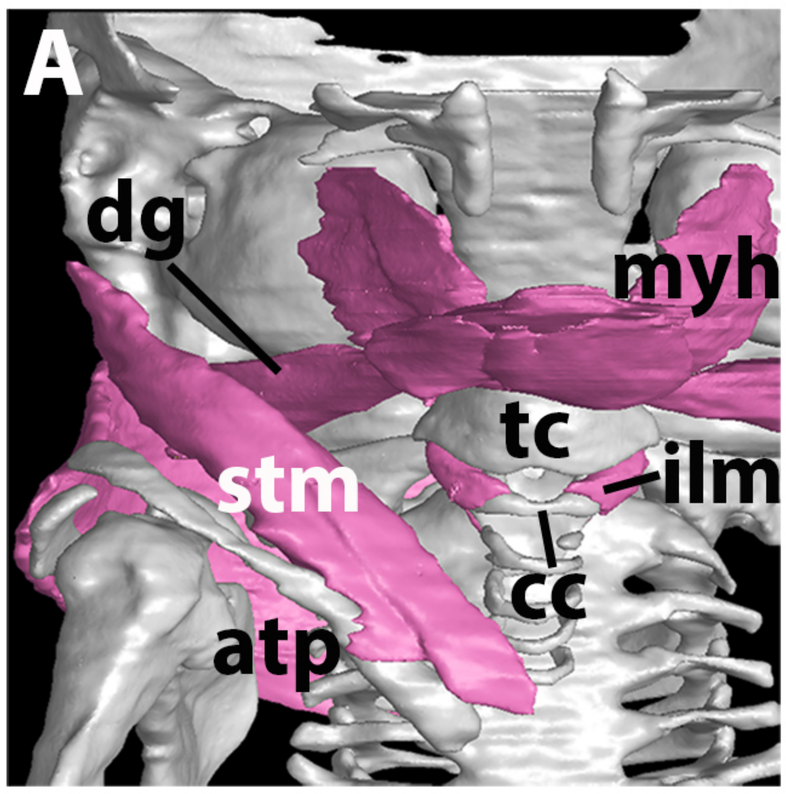

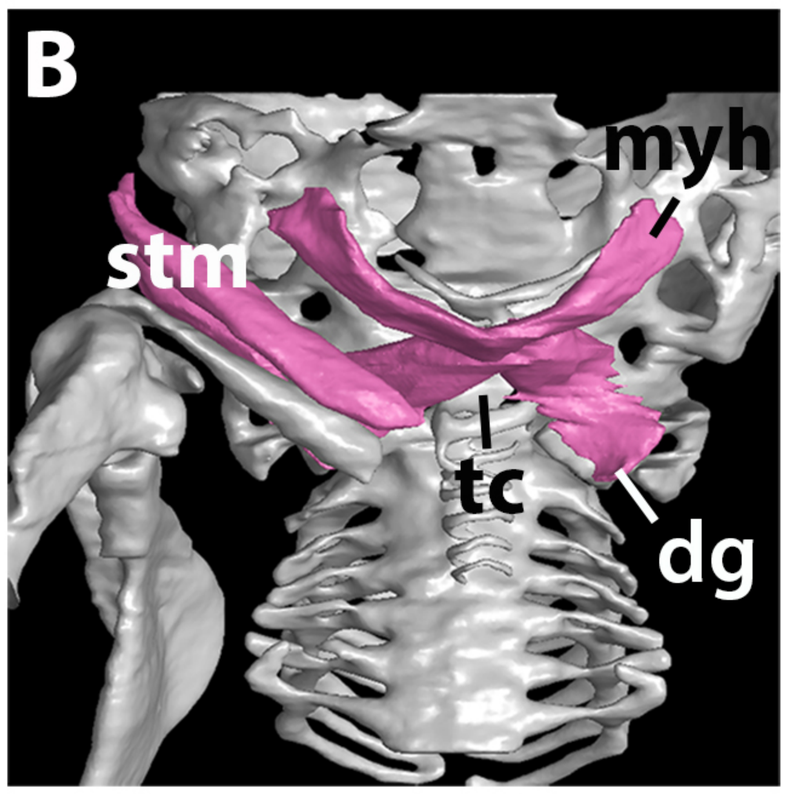

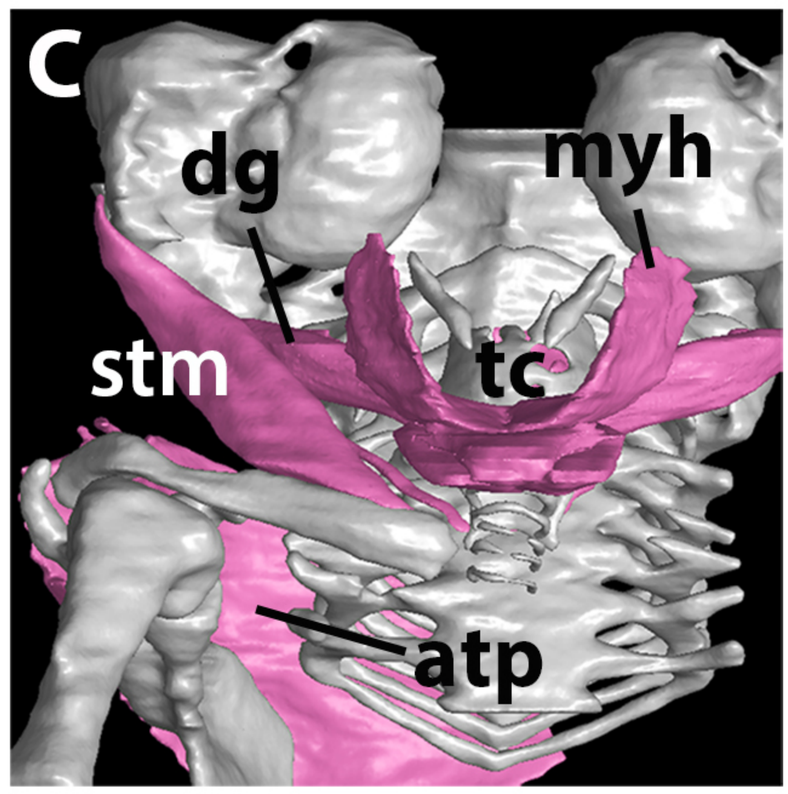

ventral

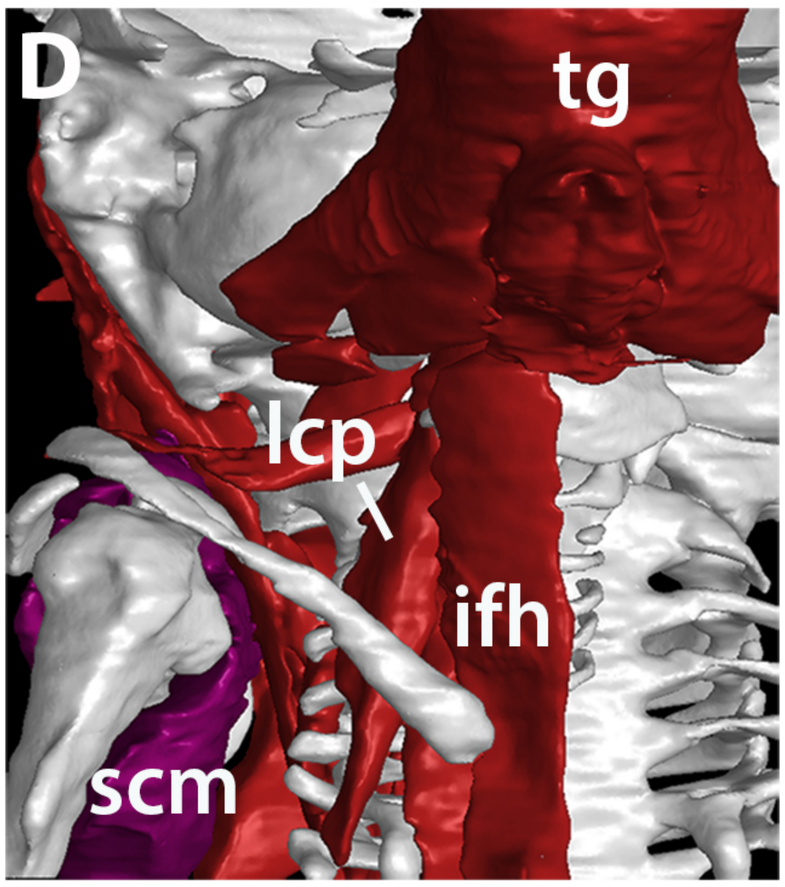

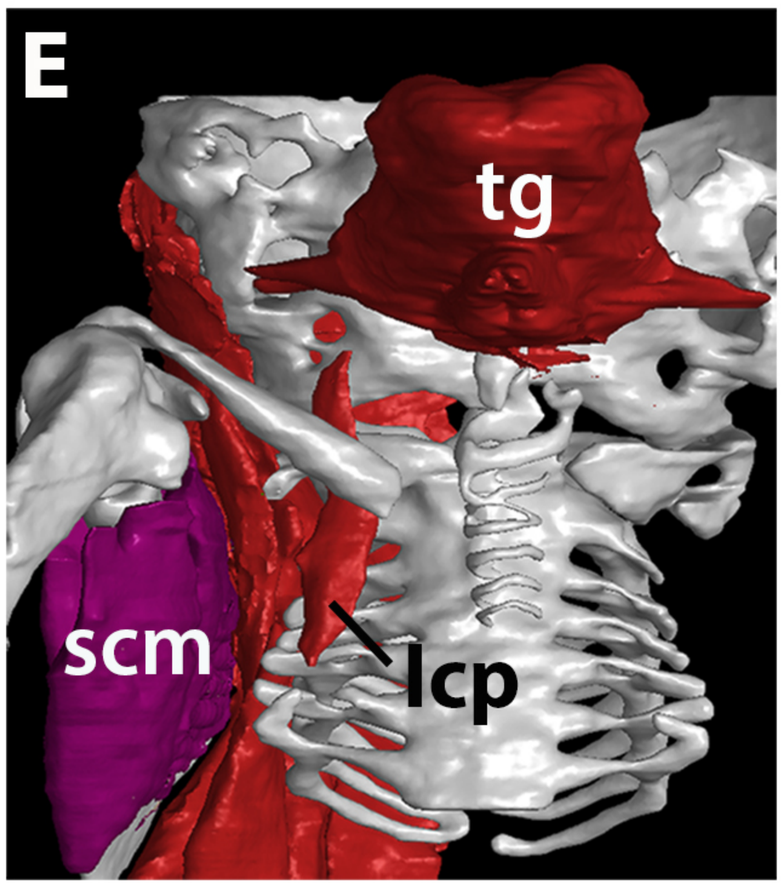

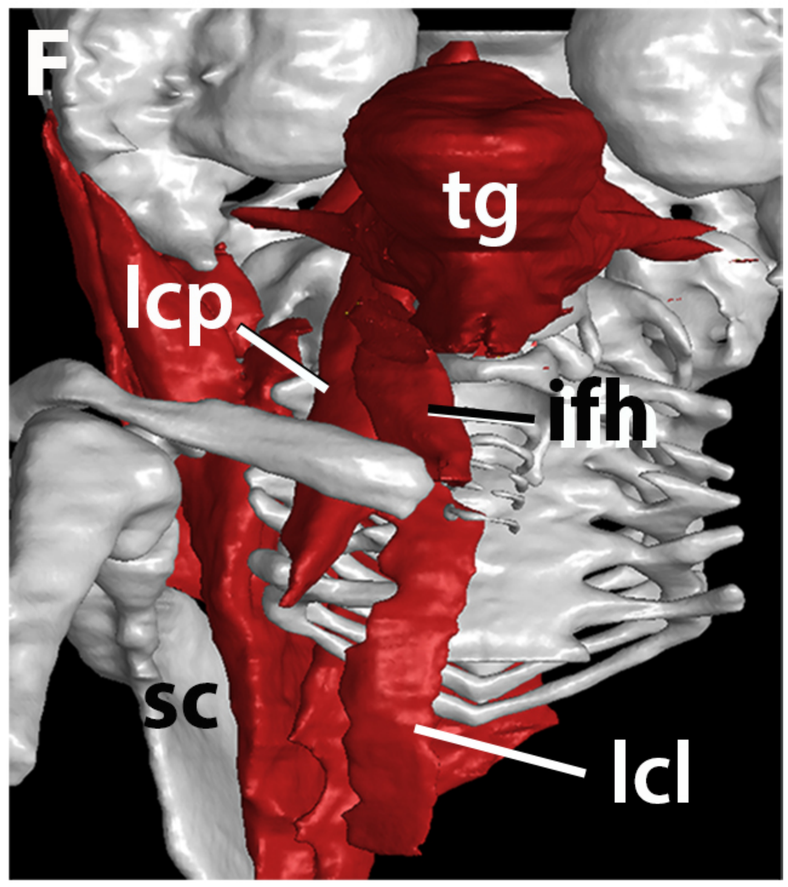

lateral

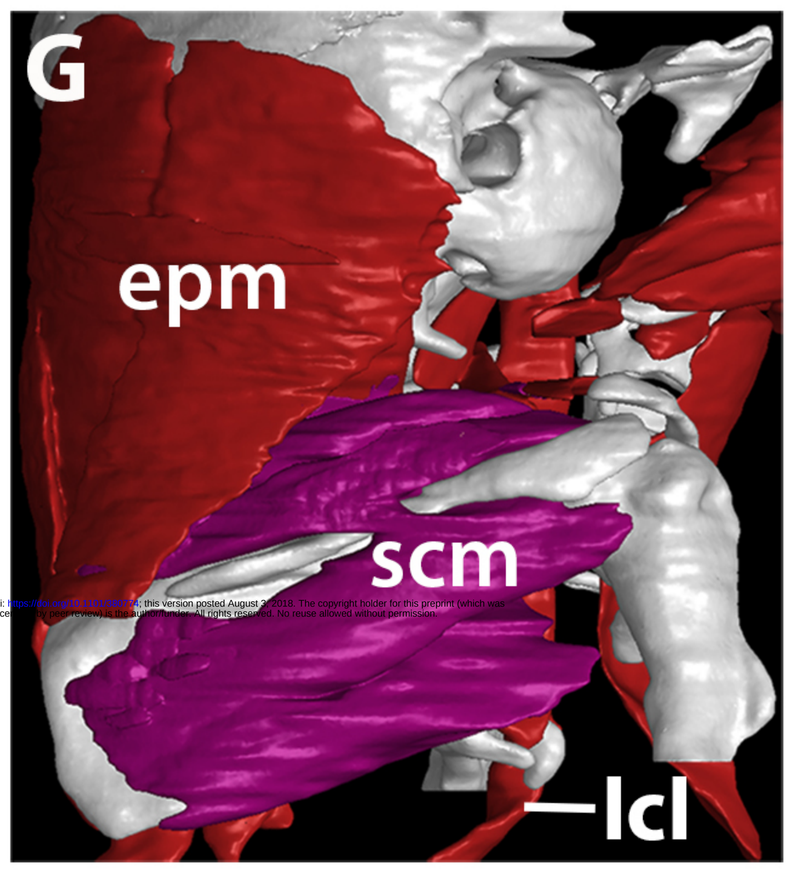

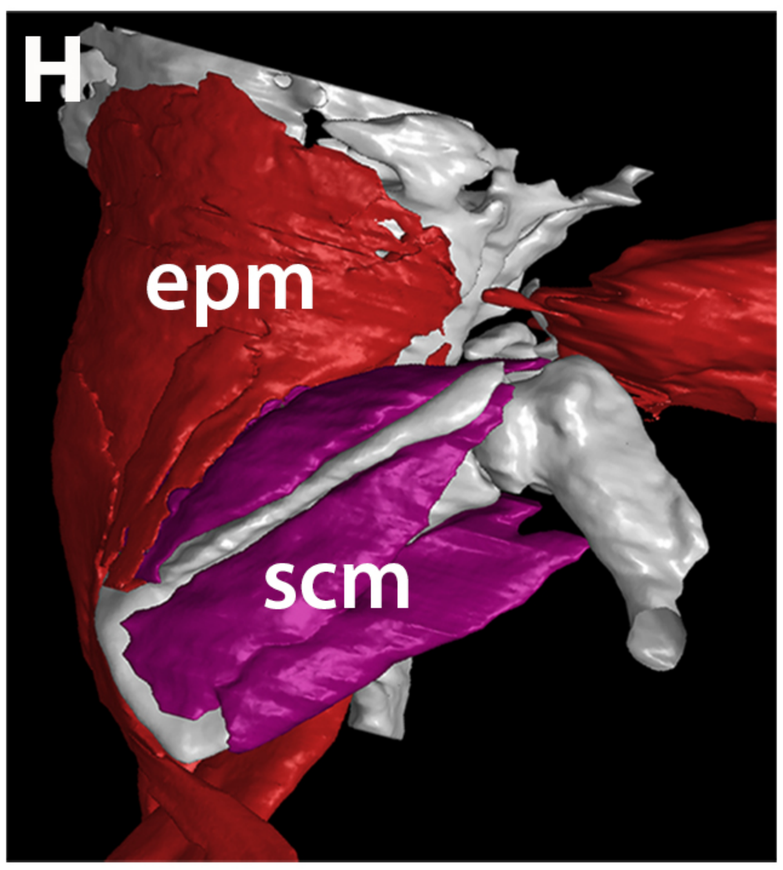

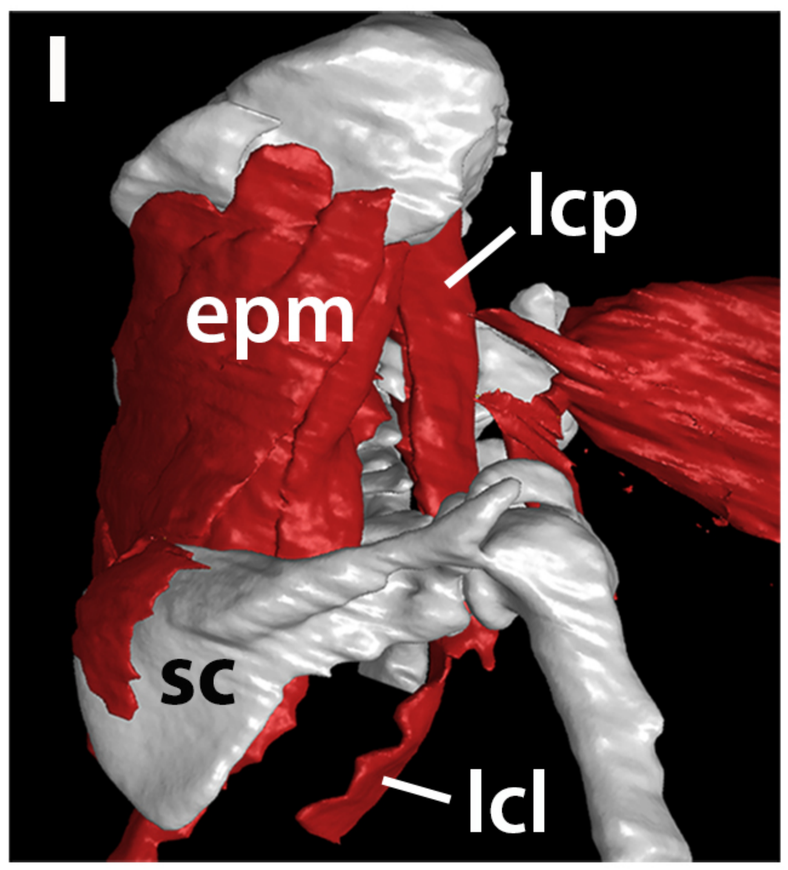

Branchiomeric program (*Mef2c-AHF/Islet1/Mesp1* lineages)

Anterior-most somitic program (*Mesp1/Pax3* lineages)

More posterior somitic program (*Pax3* lineage)

Skeletal components

Figure 6

A Hypothetical early origin

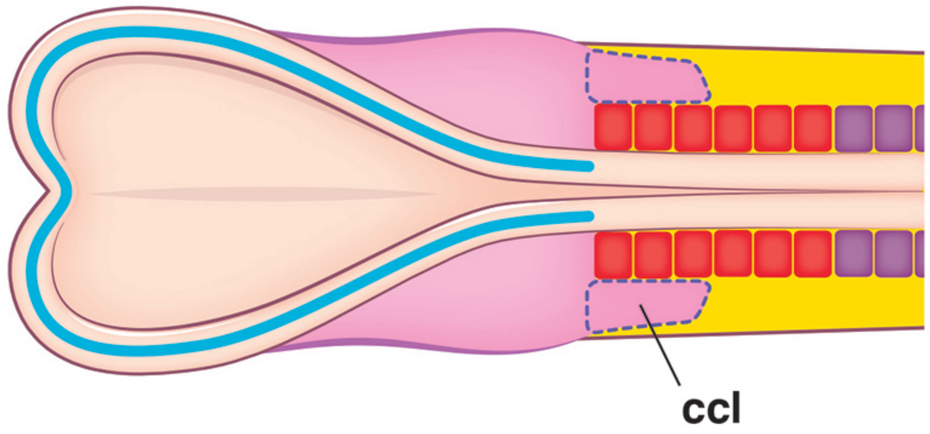

CPM : Mesp1 [1]/ Islet1 [1]/ Mef2c-AHF [1]/ Tbx1 [2]
Anterior somites : Mesp1 [1]/ Pax3 [1, 2]
More posterior somites : Pax3 [1, 2]
Cranial NC : Wnt1 [1]
LPM : Prx1 [1]

[1] Lineage analysis [2] Mutant analysis

B Embryonic derivatives

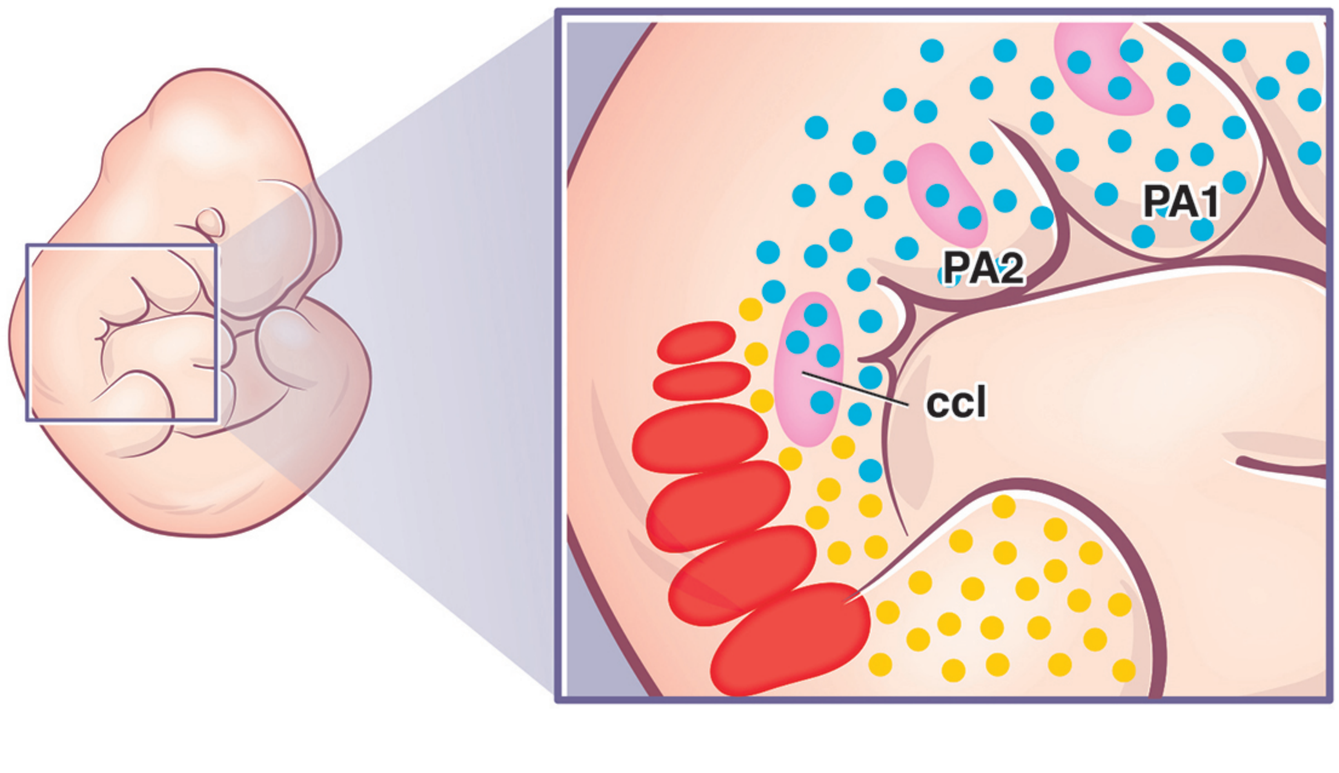

Illustrations : Cécile Mazur

C Fetal derivatives

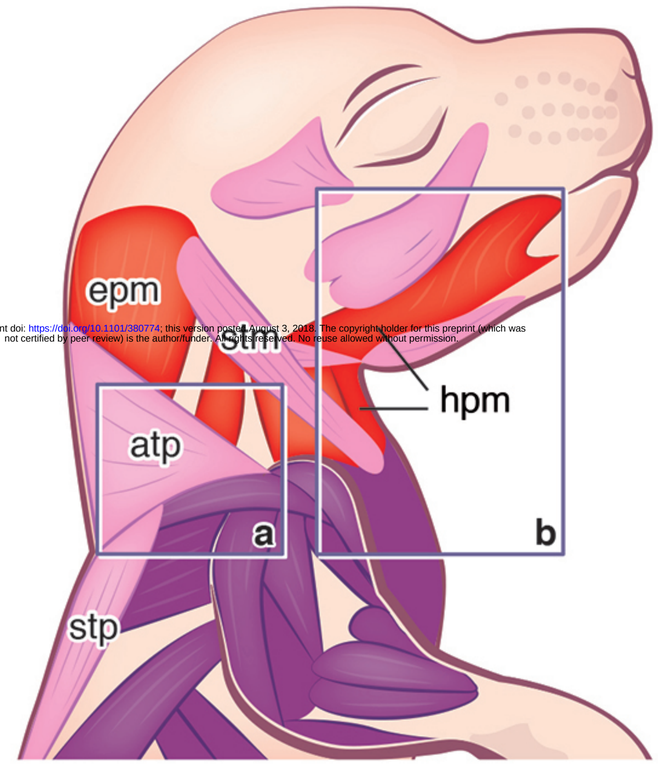

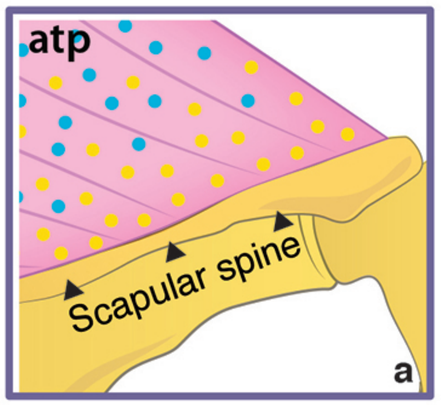

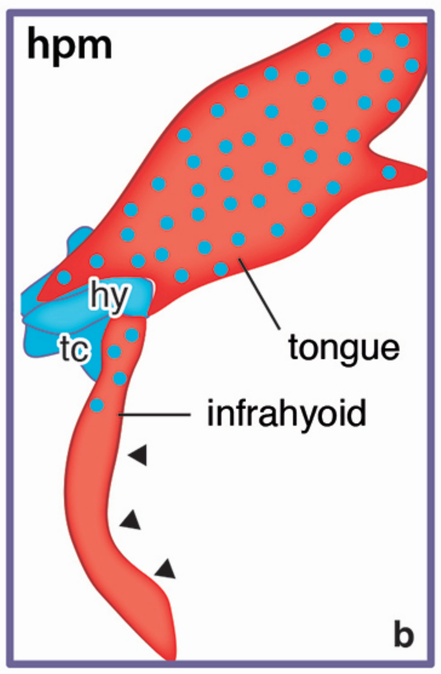

Branchiomeric muscles including cucullaris muscles
Epaxial and hypaxial neck muscles
Trunk and limb muscles
NC-derived connective tissue and skeletal components
LPM-derived connective tissue and skeletal components
▶ **No NC contribution to connective tissue and shoulder**

D Model of muscle connectivity network

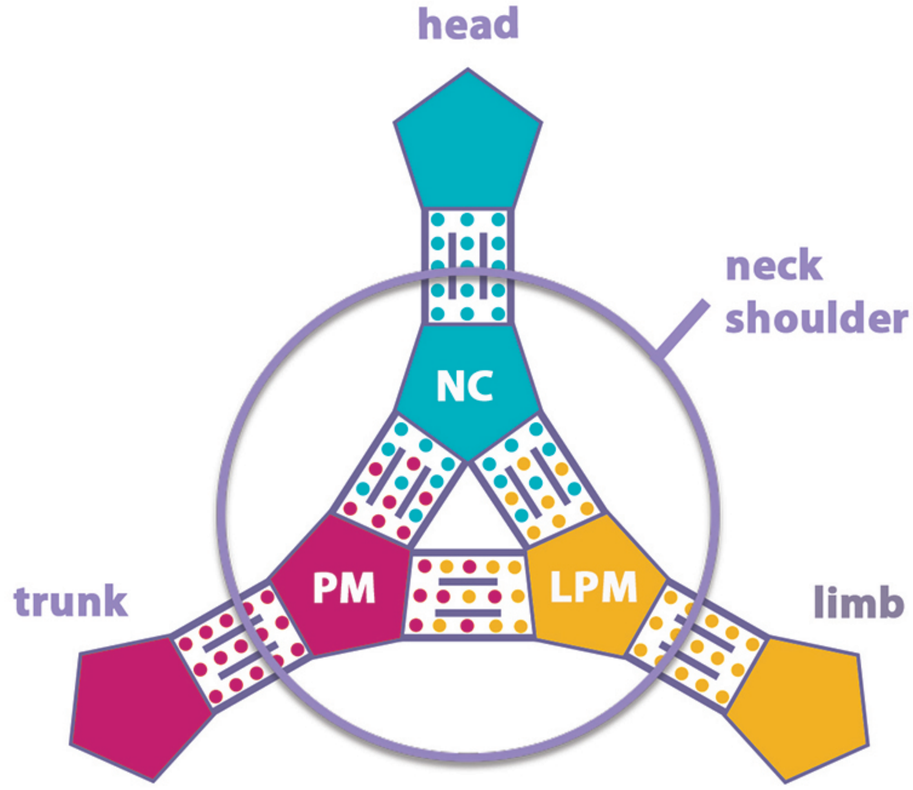

Attachment sites of NC (blue), LPM (yellow) or paraxial mesoderm (PM, purple) origin
Myofibres
Connective tissue of NC (blue), LPM (yellow) or paraxial mesoderm (PM, purple) origin

Figure 7